

University at Albany, State University of New York

Scholars Archive

Biological Sciences

Honors College

5-2010

Bioengineering Tissue Constructs Using Elastic Alginate Hydrogels

Barbana A. Graham
University at Albany, St

Follow this and additional works at: https://scholarsarchive.library.albany.edu/honorscollege_biology



Part of the [Biology Commons](#)

Recommended Citation

Graham, Barbana A., "Bioengineering Tissue Constructs Using Elastic Alginate Hydrogels" (2010).
Biological Sciences. 6.
https://scholarsarchive.library.albany.edu/honorscollege_biology/6

This Honors Thesis is brought to you for free and open access by the Honors College at Scholars Archive. It has been accepted for inclusion in Biological Sciences by an authorized administrator of Scholars Archive. For more information, please contact scholarsarchive@albany.edu.

Bioengineering Tissue Constructs Using Elastic Alginate Hydrogels

An honors thesis presented to the
Department of Biological Sciences,
University at Albany,
State University of New York
in partial fulfillment
of the Honors Program Requirements

Barbara A. Graham
May 2010

Department of Biological Sciences
University at Albany

This Honors Thesis has been read and approved
by the undersigned and is hereby recommended for acceptance.

Thesis Committee:

Research Advisor: (Name) _____

(Signature) _____

(Date) _____

Member: (Name) _____

(Signature) _____

(Date) _____

Member: (Name) _____

(Signature) _____

(Date) _____

ACTION: Accepted Not Accepted

Robert Osuna
Departmental Honors Program Director

Date

Abstract

Bioengineered 3-D tissue constructs have great potential for understanding tissue development and tissue repair in patients lacking functional organs. One of the major challenges faced in the field, however, is to build functional tissue constructs that resemble tissue found *in vivo*. Cells and tissues in the body are organized into three-dimensional architectures, which interact with fibrillar extracellular matrix (ECM) proteins at a nanoscale. Both the topology and elasticity of the ECM play critical roles in regulating tissue formation. Alginate, a naturally occurring polysaccharide, is a good candidate to use as a biomaterial to mimic the topography and elasticity of the ECM. In this study, the feasibility of synthesizing 3-D alginate microtubes, nanofibers and microbeads that simulate the elasticity and topography of the ECM has been investigated. Using a series of techniques, we fabricated tissue constructs with varying shapes, sizes, and elasticities. 3-D alginate microtubes, nanofibers, and microbeads were synthesized through the processes of microfluidics, electrospinning, and electrodroplet, respectively. The experiments conducted throughout this project provide a fundamental platform for bioengineering artificial salivary glands in future studies for patients who suffer from xerostomia (dry mouth) and salivary gland hypofunction.

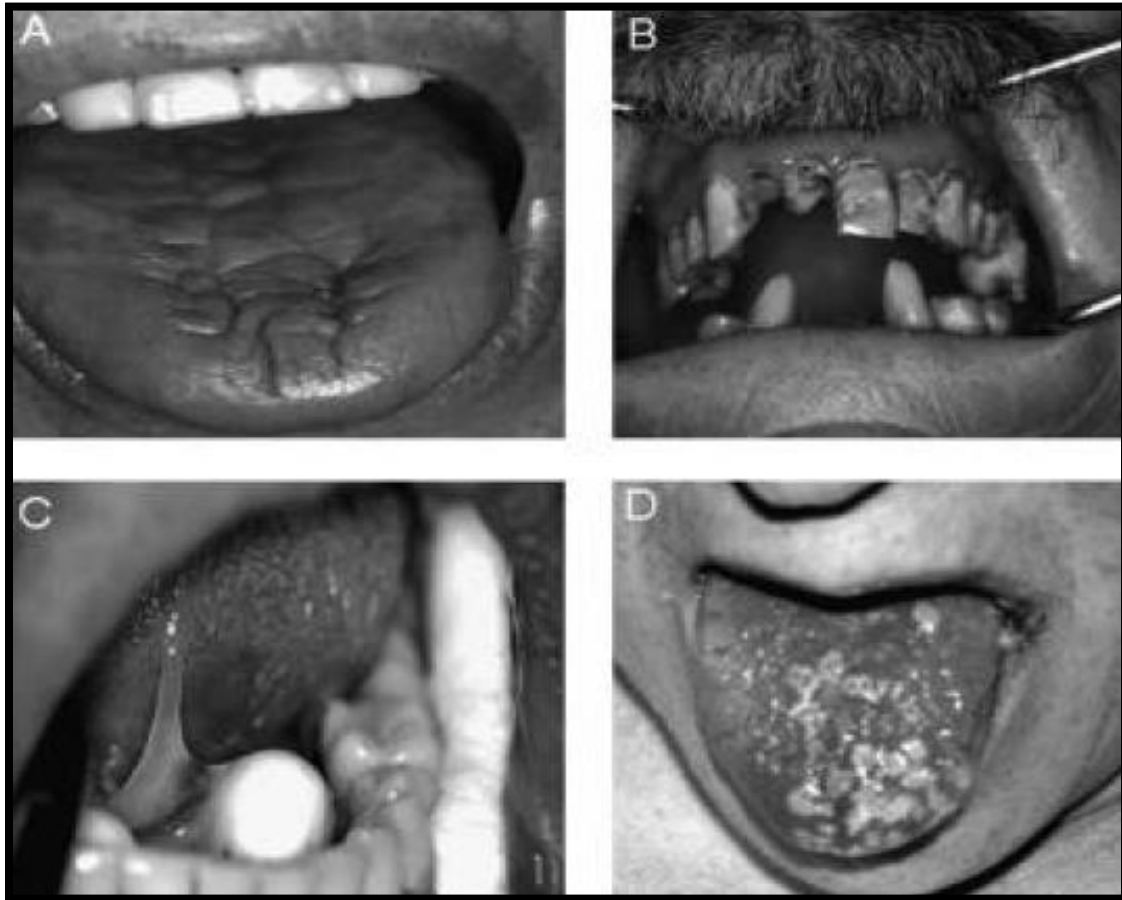
Acknowledgements

I would like to express my sincerest thanks to my advisors, Dr. Melinda Larsen, Dr. Magnus Bergkvist, and Dr. Yubing Xie for not only serving as great mentors, but also for providing me with multidisciplinary and collaborative environments to conduct my research. I appreciate the time and effort that the members from my Honors Thesis Committee, including Dr. Min-Ho Lee, spent in revising my work. I would also like to give thanks to the undergraduate and graduate students from the labs of Dr. Melina Larsen and professors from the College of Nanoscale Science and Engineering, who expressed a fervent desire to assist me with the technicalities of my project.

Introduction

Tissue engineering is an emerging field that strives to design medical devices that serve to replace, enhance, or maintain the function of tissue that has been damaged by disease or injury (Liu, et al., 2007). The multidisciplinary field is very promising for biomedical applications because it can take the place of many therapies that often lead to harmful side effects, including organ transplantation and reconstructive surgery (Wells, et al., 2006). An engineered artificial salivary gland could be helpful for treating patients who experience salivary gland dysfunction brought about by xerogenic medications, radiation therapy to the head and neck areas, diabetes, and Sjögren's syndrome (Aframian, 2008).

The aforementioned conditions can lead to a devastating disorder known as xerostomia. Xerostomia is characterized by its causation of an excessively dry mouth resulting from the reduction or absence of saliva flow (Porter, et al., 2010). Saliva is a very important component of the oral cavity because it functions to protect the mouth from infectious microbes, dangerous pH levels, and debris from leftover food (Dodd, et al., 2005). It also serves to prevent dental caries from forming and oral infections from developing. Patients who suffer from salivary gland hypofunction and decreased saliva production experience difficulties eating, tasting, communicating through speech, swallowing, and accepting dental prosthesis (Atkinson, 1994). They can often be burdened with salivary gland enlargement, sensitive nasal passages, and a perpetual sore throat. Some individuals also have an increased susceptibility to develop dental caries, thick and stringy saliva, fissures on the lips and tongue, and fungal infections such as candidiasis (Figure 1). By finding innovative ways to bioengineer artificial salivary glands, we can help improve xerostomia patients' quality of life and enhance their potential for productive living.



In humans, the salivary glands are situated inside the oral cavity. There are three major pairs of glands: the submandibular, sublingual, and parotid glands (Figure 2). There are also hundreds of minor salivary glands located throughout the mouth. Collectively, these glands contain acinar cells which are responsible for secreting one liter or more of saliva daily (Figure 3). We can strive to create constructs that simulate the function and structural components of the biological salivary gland by employing the field of tissue engineering. Throughout this study, we use micro and nano processing techniques to fabricate an emulative array of tissue constructs. For instance, the first aspect of our project involves fabricating alginate hydrogel microstrands that conspicuously simulate the hollow ducts of the salivary gland. The second aspect of this

research consists of synthesizing alginate hydrogel nanofibers that mimic the biological ECM. We are also able to imitate the acinar structures of the salivary gland by generating alginate hydrogel microbeads. By combining tissue engineering methodologies and stem cell techniques, we can eventually create an artificial device that enhances the function of impaired salivary glands (Aframian, 2008).

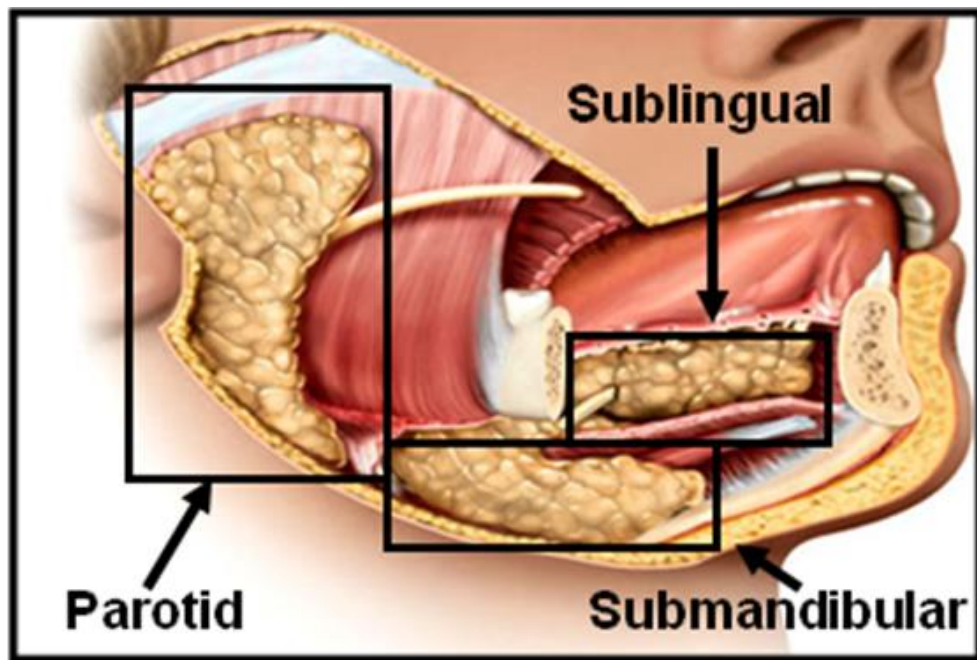


Figure 2: Locations of Salivary Glands in the Oral Cavity

The three major salivary glands of the human oral cavity are the submandibular, sublingual, and parotid glands. (Aframian, 2008).

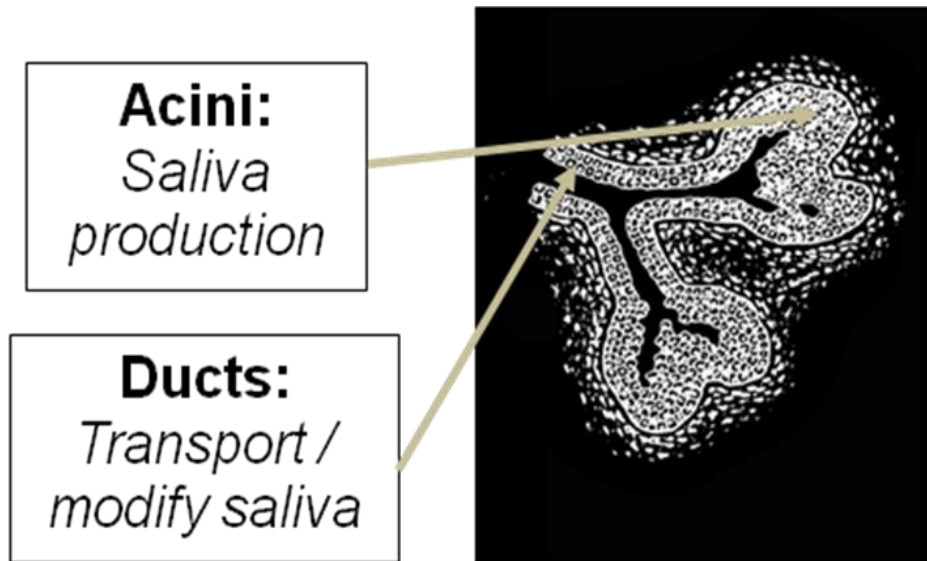


Figure 3: Components and Structure of the Salivary Gland
 Acinar cells are responsible for producing saliva. Ductal cells, which are located within the ducts, modify the saliva and carry it to different parts of the oral cavity.

Tissue engineering, in general, involves the seeding of cells onto biocompatible scaffolds (Figure 4). An idealized process of this consists of isolating cells from donor tissue, cultivating the cells *in vitro*, and allowing them to proliferate. The differentiating cells can then be seeded onto a 3-D biocompatible matrix and implanted back into the subject lacking functional tissue. Throughout my research, the model cell lines that we used as a preliminary were NIH 3T3 fibroblast cells and mouse Embryonic Stem Cells (mESCs). However, the long-term goal of this study is to ultimately create scaffolds specifically designed for the seeding of salivary gland cells. In the basic tissue engineering concept depicted in figure 4, once cells are seeded onto the scaffold, the scaffold has the ability to provide an environment that is conducive to cell proliferation and differentiation. Given the appropriate characteristics, the scaffold can also instigate the polarization and organization of cells into functional units (Gerecht-Nir, et al., 2004). We typically create the scaffolds out of hydrogel substances for a number of reasons.

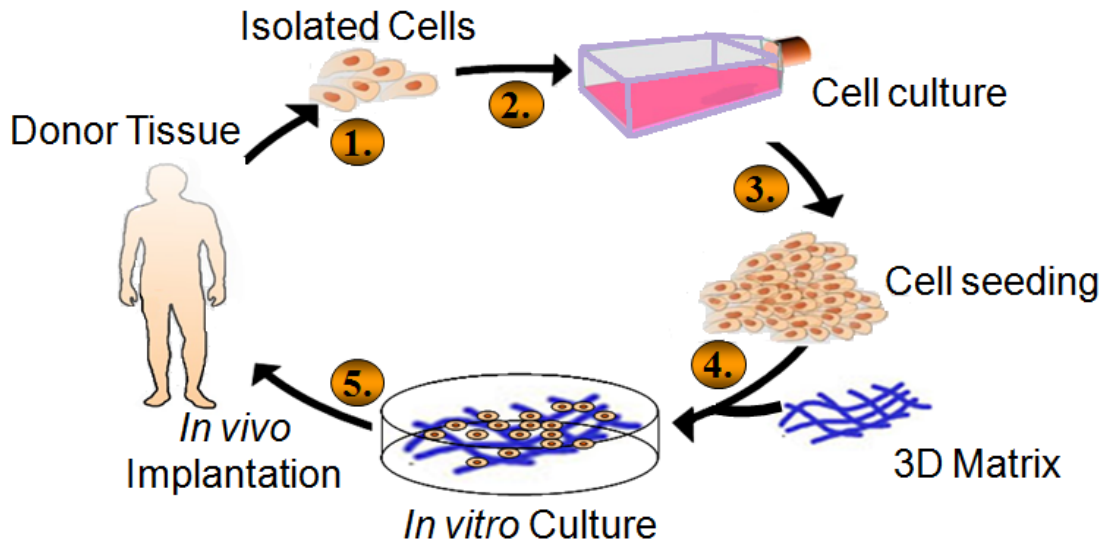


Figure 4: Basic Diagram of the Tissue Engineering Process

Cells are isolated from a donor organism and cultured *in vitro*. After the cells proliferate and differentiate into their desired lineages, they are seeded onto biocompatible matrices conducive to sustaining cell viability (George, 2009).

Hydrogel scaffolds are used for *in vitro* cell cultivation primarily because of the similarities they share with biological tissue, their ease of manipulation, mechanical stability, and their ability to allow diffusion of nutrients through hydrogel matrices. It has been shown that the elasticity of the hydrogel environment plays a critical role in maintaining cell viability and differentiation (Ahearne, et al., 2005). Hydrogel scaffolds can also have environments that vary in elasticity, ranging from being solidified to being completely liquefied (Topuz, et al., 2009). However, the scaffolds that closely resemble the natural environment found *in vivo* have a softer and more porous topography. Evidence supporting the use of hydrogels for *in vitro* cell cultivation of mouse salivary gland cells comes from a study conducted by Wei, et al. (2007). In the experiments conducted by Wei, et al., acinar cells derived from an embryonic salivary gland suspended in Matrigel, a hydrogel substance rich in laminin, were shown to reorganize into a

branched tissue aggregate resembling the biological architecture of an intact salivary gland. Additionally, the cells were shown to express differentiation markers.

We hypothesized that alginate, a naturally occurring polymer isolated from brown seaweed, would be a suitable biomaterial to engineer hydrogel tissue constructs that could be tested as scaffolds for generating artificial salivary glands. Alginate is biocompatible, non-toxic, biodegradable, and has a highly tunable elasticity (Orive, et al., 2006). In the presence of divalent cations, it is capable of forming an irreversible porous hydrogel substance. These unique characteristics render alginate very promising to use for tissue bioengineering purposes because it can simulate many characteristics of tissues found *in vivo*. Research has also indicated that alginate can provide environments that promote the growth of a variety of cell types (Gerecht-Nir, et al., 2004). We hypothesized that by attaching cells to 3-D alginate tissue constructs synthesized using novel techniques, it would be possible to create structures that resemble biological structures *in vivo*.

The chemical structure of alginate is comprised of varying ratios of α -L-guluronic acid (G) and β -D-mannuronic acid (M) residues linked by 1,4-glycosidic bonds (Figure 5). To maintain the ionic strength of alginate, sodium chloride (NaCl) is reacted with alginate to form sodium alginate ($\text{NaC}_6\text{H}_7\text{O}_6$)_n. In the presence of polyvalent cations, such as the Ca^{2+} ion from calcium chloride (CaCl_2), a cross-linking reaction occurs between aqueous alginate and aqueous calcium chloride. The cross-linking reaction induced by Ca^{2+} serves to enhance the strength of the inter- and intramolecular bonding that occur within the alginate molecule (Figure 6). In this way, alginate hydrogel is formed.

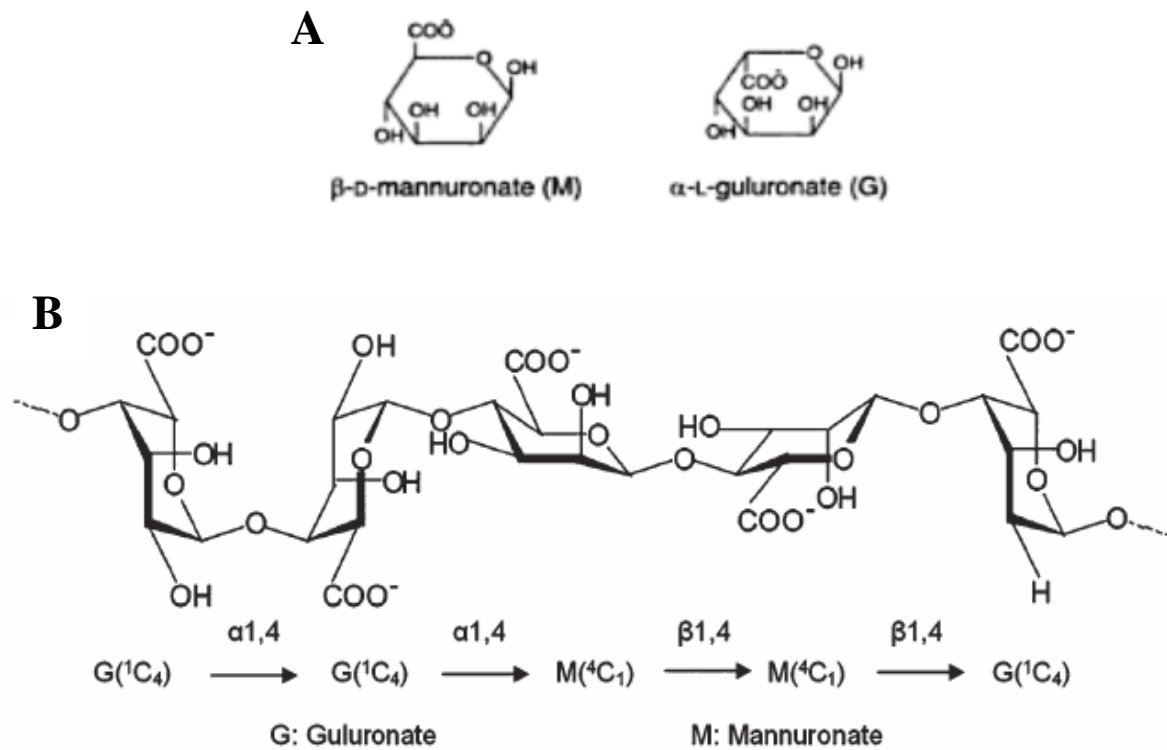


Figure 5: Chemical Structures of β -D-Mannuronic Acid (M) and α -L-Guluronic Acid (G)
 (a) Each monosaccharide residue contains highly anionic carboxylic acid groups that greatly influence the overall behavior of the polymer in solution.
 (b) G and M can form glycosidic linkages between themselves or in varying combinations with each other.

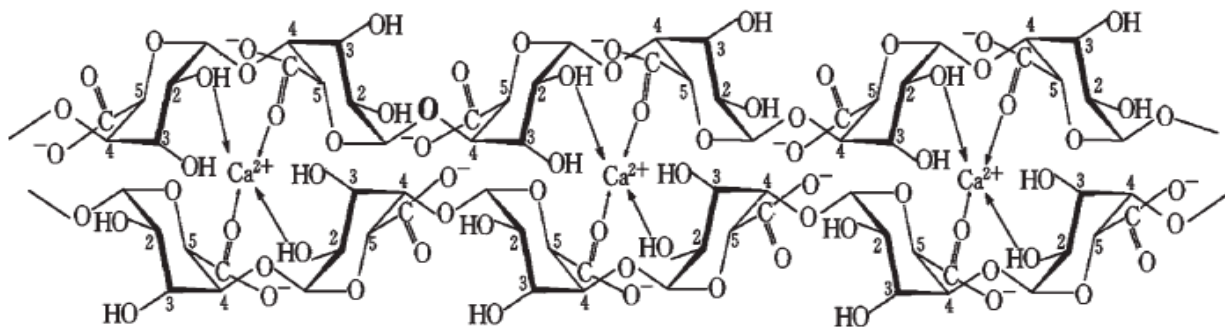


Figure 6: Chemical Structure of Alginate Cross-linked with Ca^{2+} from $CaCl_2$
 Alginate is comprised of alternating units of β -D-mannuronic acid and α -L-guluronic acid. The Ca^{2+} cross-linking reaction serves to increase the strength of the bonds that exist within the molecule.

Table of Contents

Title Page	i
Approval Signatures	ii
Abstract	iii
Acknowledgements	iv
Introduction	v
Table of Contents	xii
Chapter 1: "Fabrication of Alginate Microstrands Using Microfluidic Devices"	
Introduction.....	1
Materials and Methods.....	1
Photolithographic Patterning for MEMS Devices	1
Fabrication of PDMS Molds Using Patterened-Silicon Wafers	3
Fabrication of Agarose Molds Using Patterned-Silicon Wafers.....	5
Preparation of Alginate and CaCl ₂ Solutions	6
Encapsulation of MESC's Using SU8 Filtration Devices.....	7
Assembly of the SU8 Filter Extrusion Devices	8
Assembly of the Microfluidic "Snake Channel" Devices	9
Results.....	10
Degassing and Applying PDMS Molds	10
Applying Agarose Molds to Patterned-Silicon Wafers.....	11
Homogenizing Alginate Solutions	13
Testing the Microfluidic Devices	14
Cell Encapsulation via Passive Flow through SU8 Filters	15
Right-Side up Microfluidic Extrusion Devices	18
Microfluidic "Snake Channel" Devices	19
Discussion.....	21
Chapter 2: "Synthesis of 3-D Alginate Nanofibers using the Electrospinning Technique"	
Introduction.....	25
Materials and Methods.....	27
Preparation of Alginate/PEO Solutions.....	27
Assembly of Electrospinning Apparatus and the Synthesis of 3-D Alginate Nanofibers.....	27
Results.....	30
Effect of the Concentration of the Overall Solution	30
Effect of the Ratio of Alginate to PEO in Solution	30

Effect of the Molecular Weight of PEO	31
Effect of Viscosity on the Process of Electrospinning.....	31
Discussion	33
 Chapter 3: "Fabrication of 3-D Alginate Microbeads Using the Electrodroplet Technique"	
Introduction.....	35
Materials and Methods.....	39
Preparation of Sodium Alginate Solutions	39
Assembly of Electrodroplet Apparatus and the Synthesis of 3-D Alginate Microbeads	40
Application of Outer Surface Coatings	41
Cell Passaging.....	44
Immunocytochemistry of Fibronectin-Coated Microbeads.....	44
Attachment of Cells to Outer Membrane of 3-D Alginate Microbeads	45
Results.....	46
Mouse Embryonic Stem Cells as a Model Cell Line	46
Effect of Multilayer Surface Coats on 3T3 Fibroblast Cell Adhesion	47
Optimization of Fibroblast Cell Adhesion using Different Surface Coats	47
Effect of Incubation Time on Fibroblast Cell Adhesion.....	49
Syber Green and Rhodamine-Phalloidin Fluorescent Staining	51
Immunocytochemistry of Fibronectin-Coated Microbeads	52
Optimization of SIMS Cell Adhesion using Different Surface Coats	53
Discussion	54
Conclusions.....	56
References.....	59

Chapter 1:

“Fabrication of Alginate Microstrands Using Microfluidic Devices”

Introduction

From the advent of this study, we have been attempting to use a variety of techniques to engineer 3-D alginate tissue constructs in multiple configurations for the eventual application into an artificial salivary gland. Alginate, the sodium salt of alginic acid, is the natural biomaterial that we used throughout this project to create our hydrogel matrices. This chapter specifically focuses on the use of microfluidic devices to create tubular structures, or microstrands/microtubes, which might mimic salivary gland ducts *in vivo*.

To fabricate the microfluidic devices necessary for the synthesis of our hydrogel scaffolds, we initially used a process called photolithography to engrave topographic features of SU8 photoresist on a silicon wafer. This master silicon wafer was used as the template mold for the devices. Ultimately, we were trying to create microtubes smaller than 100 μ m in diameter. To control the diameter of the microstrands, we used various types of devices created through traditional Microelectromechanical Systems (MEMS) applications. After using the MEMS devices to fabricate the microstrands, the tubular constructs were gelled by cross-linking them with aqueous calcium chloride. Alginate microtubes were produced at the end of this study.

Materials and Methods

Photolithographic Patterning for MEMS Devices

Using prevailing photolithography technology, negative SU8-50 photoresist (MicroChem, Massachusetts, United States) was used to engrave topographic features onto pre-cleaned silicon wafers. Before employing the technology, the silicon wafers were cleaned in a

200mL solution of Piranha Clean (150mL sulfuric acid (H₂SO₄) and 50mL hydrogen peroxide (H₂O₂)). After applying the Piranha Clean treatment, the wafers were transferred to a sterile storage container and rinsed thoroughly with distilled water for 1 – 2 minutes. A nitrogen air gun was then used to dry the clean wafers.

After individually centering the wafers onto a spin coater one at a time, SU8 photoresist material was carefully poured onto the wafer to cover approximately ½ - ¾ of its surface. Two different speeds were used to spin the wafer to attain a final desired film thickness of 100µm. The first speed was set to 500rpm for 10 seconds with a ramp speed of 100rps to yield a resultant film thickness of ~200µm. The second speed was set to 1000rpm for 45 seconds with a ramp speed of 300rps to obtain the final surface thickness of 100µm (Figure 7). These steps were repeated for subsequent wafers. Directly following the spin coating protocol, the SU8 wafers were baked on a hot plate for 10 minutes at 65°C.

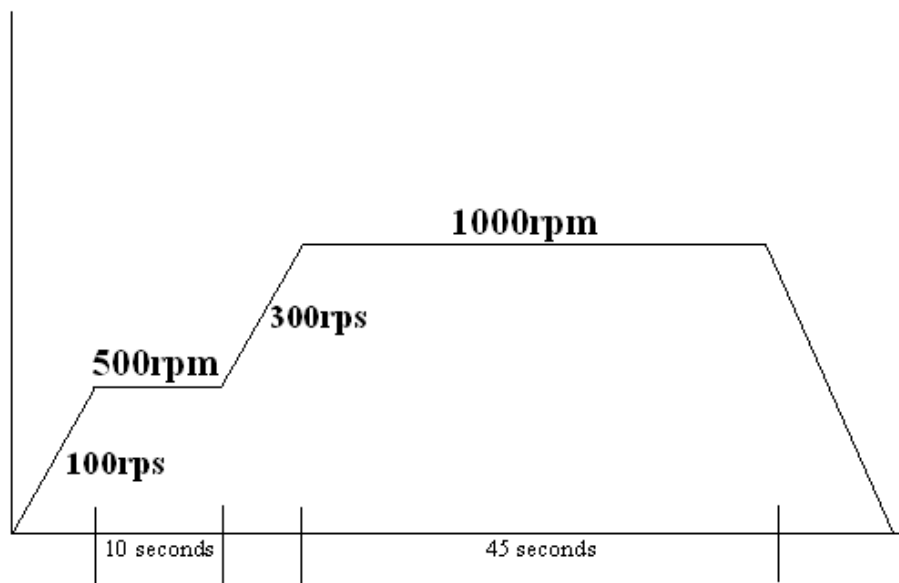


Figure 7: Varying speeds at which the SU8 Photoresist was Spin-Coated onto Silicon Wafers
Two different speeds, 500rpm and 1000rpm, were used to obtain a final film thickness of 100µm on the surfaces of each individual wafer.

To engrave topographic features onto the coated silicon wafer, a patterned-mask was used to expose specific surfaces on the wafer. To begin, the mask was mounted onto a glass plate and taped down. The glass plate and SU8 wafer was loaded into the EVG-640 Mask Contact Aligner. Using the Mask Aligner software program on the computer, an exposure time of 150 seconds was chosen. After exposing the surface of the wafer to light, we baked it on a hot plate again for 1 minute at 65°C; and then directly onto a different hot plate for 10 minutes at 95°C. We closely monitored the baking times and temperatures to avoid cracking upon cooling.

After the wafers were thoroughly cooled to room temperature, we developed the SU8 wafers in standard SU8 developer for 5 minutes or until all of the photoresist had dissolved from the surface. The photoresist on the wafer that was exposed to light through the patterned-mask was cross-linked. As a result, it was not affected by the SU8 developer and remained intact throughout the treatment. Once all of the unexposed photoresist was removed, the master silicon wafer was rinsed with isopropanol (IPA) and dried with a nitrogen air gun.

Fabrication of PDMS Molds Using Patterned-Silicon Wafers

A mixture of PDMS (polydimethylsiloxane) elastomer base and its curing agent (Dow Corning Corporation, Michigan, United States) was prepared by combining 50g of the elastomer base with 5g of the curing agent, resulting in a final ratio of 10:1. We poured the mixture on top of the topographically-patterned master silicon wafer contained in a sterile petri dish. The final assembly was placed into a vacuum chamber without the petri dish lid for 10 minutes to degas/remove excess air bubbles that were introduced during the addition of the curing agent. The assembly of the silicon wafer and PDMS was removed from the vacuum chamber, and placed into a curing oven for approximately 1½ hours at 60°C.

After using a scalpel to cut around the perimeter of the wafer and carefully removing the imprinted molds (each wafer contained five complete microfluidic devices patterns), the PDMS was placed face-down on transparency film to reduce exposure to dust in the air. The molds were oxygen plasma-treated face-up on glass slides for about 20 seconds to improve adhesion of the PDMS to the glass slides. Following plasma treatment, each mold was attached face-down to clean glass slides; and air bubbles were removed by gently squeezing tweezers against the top of the mold. The complete mold assembly was placed in the curing oven at 60°C for 30 – 50 minutes, or until applying gentle pressure no longer removed PDMS from the glass slide.

While the PDMS molds were curing in the oven at 60°C, a small amount E – 120HP Hysol® Epoxy adhesive (Loctite Corporation, U.S.A) was squeezed out of the gun onto a piece of transparency film in a small Petri dish. A stir stick was used to mix the epoxy resin together until the two yellow and white colors were thoroughly blended. We set the resin aside and allowed it to slightly harden at room temperature for 45 minutes to increase its viscosity. Once the epoxy resin was finished hardening and the curing of the PDMS molds was complete, we used a pair of tweezers to insert tygon tubes into the three channels of the PDMS mold (Figure 8).

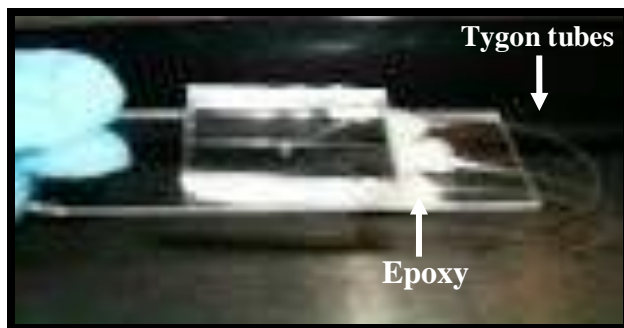


Figure 8: Complete Microfluidic Device made from PDMS. The three inlet channels contain tygon tubing adhered together via epoxy glue.

Stainless steel tubing, with tygon tubing attached, was inserted directly into the two outer channels designated for the entrance of CaCl_2 (SIGMA-Aldrich, Inc., Montana, United States). Polyimide tubing, also with tygon tubing attached, was inserted into the middle channel designated for the entrance of alginate. Tygon tubing is very flexible. Therefore, inserting the tygon tubes directly into the PDMS devices became tedious and difficult. These additional connector tubes were included with the tygon tubing to enhance the ease at which we fabricated the devices. After a tube was inserted into each of the three inlet channels, the sharp end of a stir stick was used to glue the tubes in place and to seal any openings. To help increase the efficiency of this process, we used an inverted microscope. The glued device was allowed to set overnight before it could be of any use.

Fabrication of Agarose Molds Using Patterned-Silicon Wafers

In addition to PDMS, agarose, a polysaccharide obtained from agar, was molded using silicon wafers with topographic features. This particular type of device functioned via capillary action through hydrophilic surface interactions. A solution of 2% agarose was heated to a clear liquid in a microwave oven for 35 seconds. The agarose was poured on top of a master silicon wafer containing topographically-engraved features. The assembly was allowed to cool at room temperature for 5 – 10 minutes, or until it hardened and turned more opaque. The agarose mold was carefully lifted from the silicon wafer and placed face-up on a glass cover slip (Figure 9). During this process, it was imperative to be gentle while removing the agarose mold from the wafer to avoid breakage. Thereafter, a drop of alginate was added to the top of one of the channel openings and allowed to travel up toward the 3-way junction located at the middle of the device.

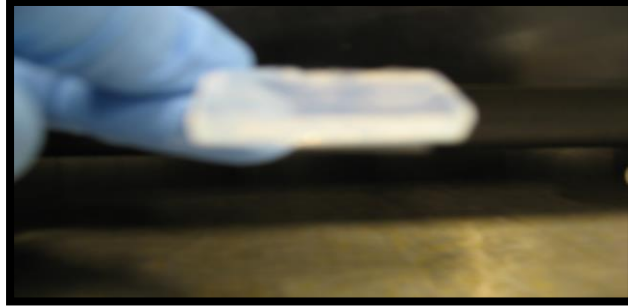


Figure 9: Complete Microfluidic Device made from Agarose. This fragile agarose assembly is supported by a glass cover slip.

Preparation of Alginate and CaCl₂ Solutions

To maintain the ionic character of alginate, aqueous solutions of 0.9% sodium chloride (SIGMA-Aldrich, Inc., Montana, United States) were prepared by adding 0.225g of NaCl to 25mL of distilled water (dH₂O). CaCl₂ solutions were prepared by adding 1g of CaCl₂ to 50mL of dH₂O to yield a final concentration of 2%. Five solutions of 0.06%, 0.5%, 1%, 1.5%, and 2% of low viscosity (250cp) alginate (SIGMA-Aldrich, Inc., Montana, United States) were prepared by mixing 5mL 0.9% NaCl with different amounts of alginate (Table I).

We then filtered the solutions to remove large particles such as bacteria, and to sterilize the alginate. We began the sterilization process by first using disposable filters of pore size 0.8 μ m. The alginate solutions were loaded into a sterile syringe and extruded through the filter and into a sterile container. The 0.8 μ m filtered solution was then filtered using sterile filters of 0.45 μ m and 0.2 μ m pore sizes sequentially. To ensure sterility and to avoid contamination, the 0.2 μ m filtration process was completed under a biosafety cabinet with constant air flow.

Table I: Description of the Protocol Used to Prepare Alginate Solutions

Overall Solution Concentrations of Alginate	Alginate (g)	0.9% NaCl (mL)
2%	0.1g	5mL
1.5%	0.075g	5mL
1%	0.05g	5mL
0.5%	0.025g	5mL
0.06%	0.003g	5mL

Previous studies indicated that the ideal solution concentrations of alginate to use for MEMS applications range from 0.06% to 2% (unpublished work, Bergvist, M., Xie, Y.).

Encapsulation of MESCs Using SU8 Filtration Devices

MESCs were cultured as described in the cell passaging protocol (see Materials and Methods, chapter 3). After centrifugation and removal of the supernatant, approximately 1mL of sterile, filtered alginate was used in place of media to resuspend the pellet of cells. While still working under the biosafety cabinet, a small petri dish was filled with 2% CaCl₂. Using a pair of tweezers, an SU8 filter containing twelve units of angled pores was placed on top of the CaCl₂ solution in the petri dish (Figure 10). A drop of alginate containing cells was placed onto each of the twelve porous units and allowed to flow passively through the pores on the filter.

Using a pipette, the CaCl₂ was aspirated from the petri dish. The SU8 filter and alginate microfibers/microtubes were left behind. 1mL of 0.05% poly-L-lysine hydro bromide in 0.9% NaCl was added to the petri dish containing the fibers. The polylysine was allowed to incubate with the microfibers for 5 minutes to ensure complete coating. The polylysine was carefully aspirated to avoid suctioning the encapsulated cells. 1mL of 0.6% sodium citrate

($\text{Na}_3\text{C}_3\text{H}_5\text{O}(\text{COO})_3$) was used to liquefy the inside of the alginate microfibers. Lastly, 0.5mL of mESC media was added to the assembly to assist in the cultivation of the encapsulated cells.

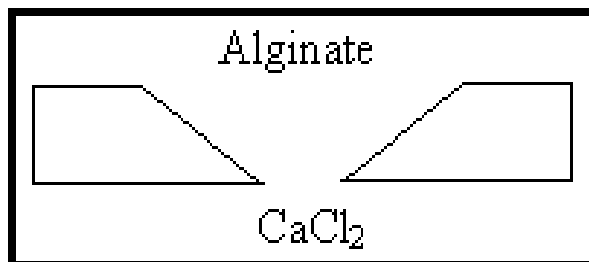


Figure 10: Cross-section of an SU8 pore. The pore is angled to ease the passive flow of alginate into the CaCl_2 curing solution.

Assembly of the SU8 Filter Extrusion Devices

An SU8 filter was placed on a PDMS mold to create a microfluidic device that operated via manual extrusion of alginate. After the PDMS mold was casted as described in the aforementioned procedure, a large hole was cut out from the PDMS; and the pores on the SU8 filter were made to line up with the larger hole on the PDMS. Sodium alginate was taken up into a syringe, and the syringe was attached to the opening of the microfluidic SU8 device. A syringe pump controlled the rate at which the sodium alginate traveled toward the SU8 filter. Once the alginate reached the SU8 filter, hydrogel microfibers began to form in the CaCl_2 curing solution (Figure 11). A right-side up version of this device was also created. It functioned by an upward flow of alginate through the SU8 filter pores. When the alginate microfibers were extruded through the pores, they were confronted with a solution of CaCl_2 to retain the hydrogel form (Figure 12).

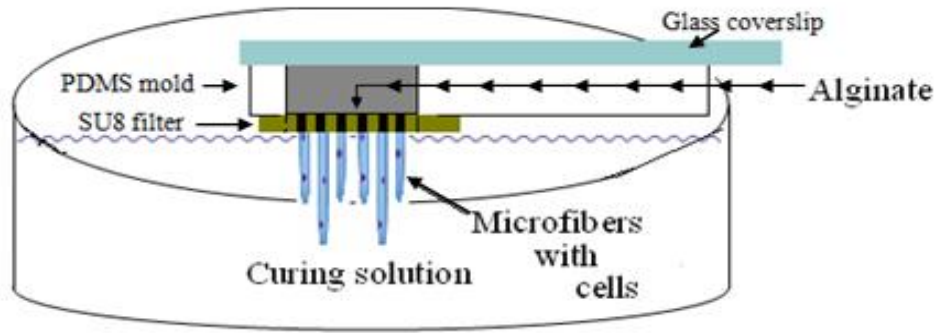


Figure 11: SU8 Microfluidic Extrusion Device Submerged Upside Down in CaCl₂. This is done to improve the flow of alginate through the pores of the SU8 filter (unpublished work, Bergkvist, M. (2009))

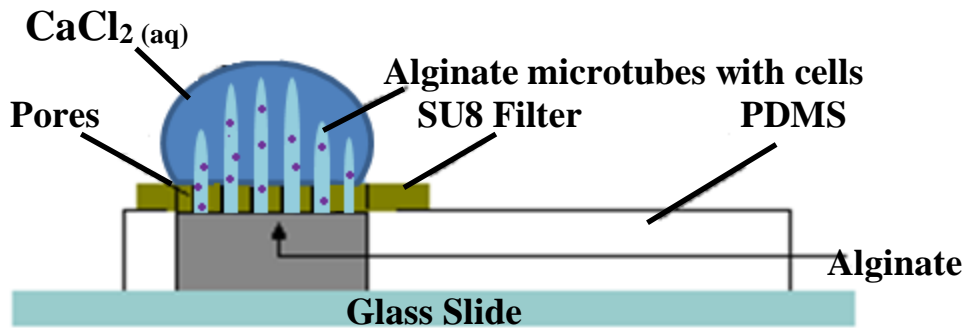


Figure 12: Cross-section of Right-Side up Active Microfluidic Extrusion Device Sodium alginate is pumped through a channel toward the SU8 filter. When alginate and CaCl₂ react, long microfibers with cells protrude from the filter.

Assembly of the Microfluidic “Snake Channel” Devices

In addition to the 3-D alginate microfibers synthesized in the previous experiments, we also discovered a novel technique to create spherical alginate microbeads of controlled size. We used a microfluidic “snake channel” approach (Figure 13). In this method, a 3-way syringe pump was attached to the three inlet channels designated for CaCl₂, sodium alginate, and mineral/corn oil. When the syringe pump was turned on, the alginate solution merged together with the oil in the adjacent channel. This caused the alginate to attain the shape of spherical

microbeads of uniform size. The microbeads were then cross-linked with CaCl_2 as they traveled through the remainder of the channel. The sizes of the microbeads were carefully controlled by monitoring the rates at which each substance flowed through the device. Optimal pump rates were between $5\mu\text{L}/\text{min}$ and $15\mu\text{L}/\text{min}$.

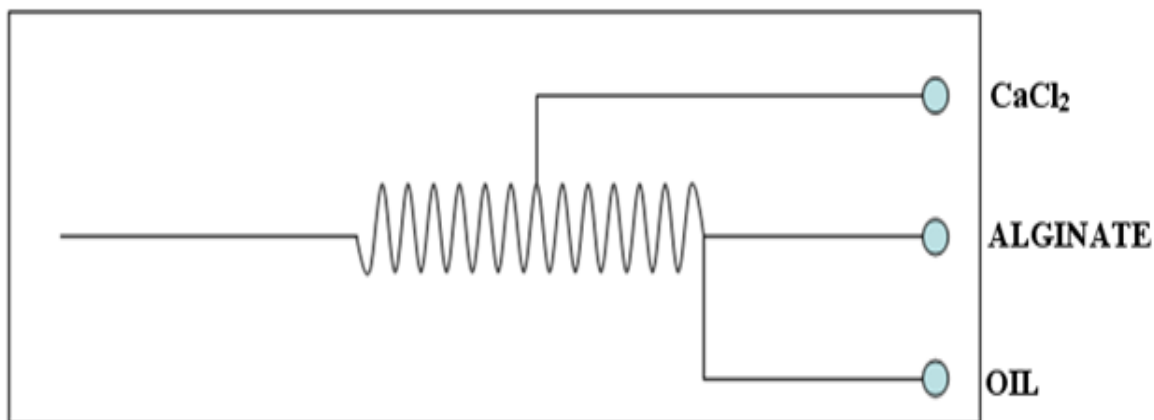


Figure 13: Microfluidic “Snake Channel” Device

This device can be used to control the size of alginate microbeads (unpublished work, Bergkvist, M., 2009).

Results

Applying PDMS Molds to Patterned-Silicon Wafers

Upon mixing the PDMS base with curing agent in a 10:1 ratio respectively, we found that air bubbles formed in the solution. Although a few small air bubbles in PDMS solution was acceptable, the presence of copious amounts would hinder the fabrication of the microfluidic devices. Therefore, we had to degas the PDMS mixture in a vacuum chamber for 10 minutes to remove the excess air bubbles. Leaving the PDMS in the vacuum chamber for too long would cause the solution to reach a high viscosity at which the air bubbles would not float to the surface when poured onto the master mold. We also found that in order to prevent the bubbles in the

solution from boiling over the petri dish while in the vacuum chamber, we had to allow small amounts of air into the chamber every 3 minutes. However, to avoid having to stop the vacuum suction every 3 minutes, we mixed the PDMS and curing agent together in a larger container. We used a disposable plastic cup to carry out this reaction, and then we proceeded to degas the mixture in a weak vacuum chamber before applying it to the master silicon wafer. By doing so, the bubbles would increase in size but not boil over the side of the container as they did in the petri dish (Figure 14). We discovered that after the removal of air bubbles in the chamber, the vacuum valve had to be released slowly to prevent the sudden rush of air from knocking over the solution in the plastic cup. After pouring the degassed solution onto the topographically-patterned silicon wafer and curing it in an oven, the PDMS mold hardened. The complete, solid PDMS mold contained the desired pattern of channels. These patterns were cut out, and bonded to glass slides via plasma treatment to seal the channel openings.

Degassing and Applying Agarose Molds

Agarose was also used as a mold for the master silicon wafer patterns. However, the agarose microfluidic devices differed greatly from those made from PDMS because they did not require an external force to facilitate the flow of alginate through the channels. Instead, the agarose device functioned via hydrophillic capillary action. The most difficult challenge faced throughout this fabrication process, however, was to avoid breaking the device when handling with tweezers. The tweezers were needed to remove the patterned agarose mold from the master wafer and place it onto a glass slide for further experiments (Figure 15).

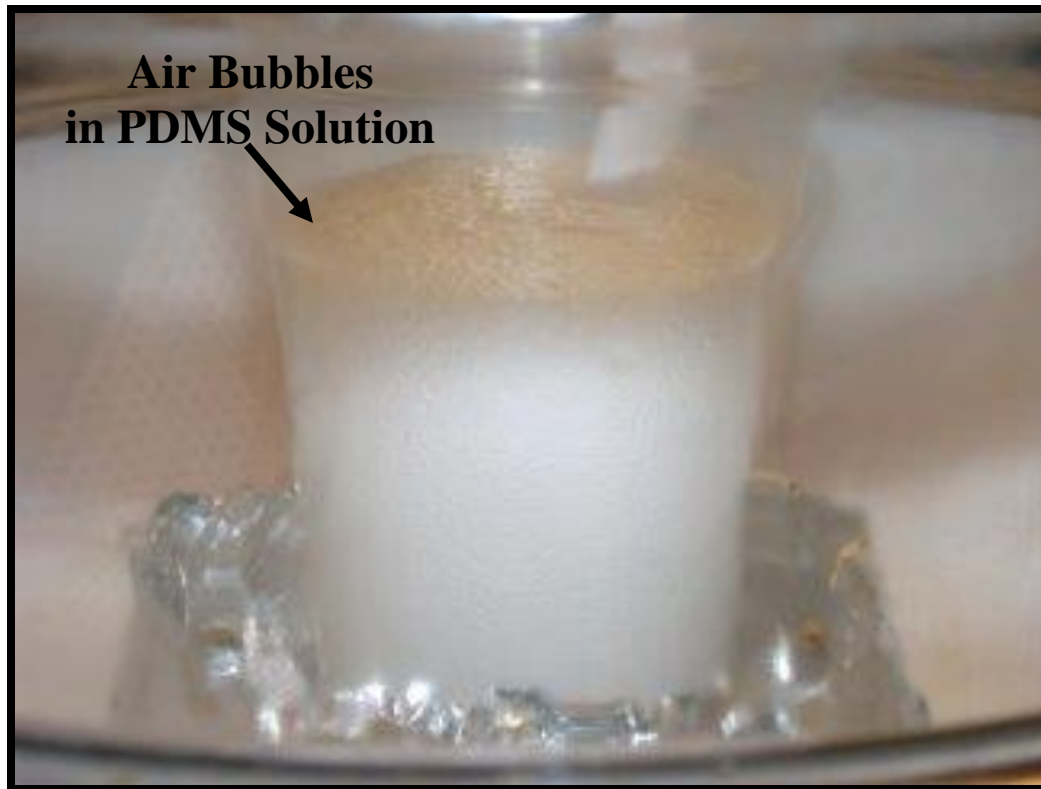


Figure 14: PDMS Solution in Vacuum Chamber

The air bubbles can be seen boiling within the container during vacuum desiccation (Lam, et al.).

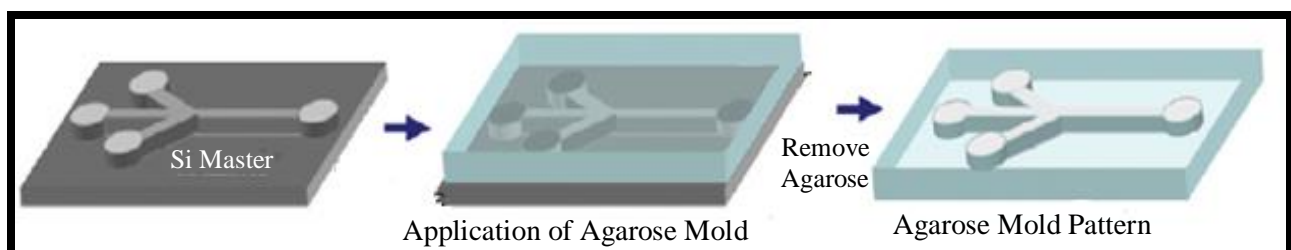


Figure 15: Applying Agarose Mold to Patterned-Silicon Wafers

The agarose is heated and added to the master silicon wafer. When the assembly is allowed to cool to room temperature, it hardens; therefore leaving behind a patterned-agarose mold.

Homogenizing Alginate Solutions

Before the microfluidic devices could be used for cell encapsulation, the sodium alginate solutions had to be prepared properly. The consistency and purity had to be monitored throughout this project because the hydrogel serves to provide a suitable microenvironment for viable cells to thrive. One of the major challenges we faced with the hydrogel substance, however, was that as the viscosity of the solution increased, so did the difficulty of obtaining pure homogeneous solutions. The 0.06%, 0.5%, and 1% sodium alginate solutions readily dissolved after using a vortex to mix them. However, we found that as we prepared solutions of higher concentrations, 1.5% and 2%, it took a longer time for the solutions to dissolve entirely after vortexing. To enhance the dissolution rate of the sodium alginate in 0.9% NaCl solution, we used a magnetic stirrer overnight. This simple technique appeared to greatly improve the consistency of the alginate hydrogel solutions (Figure 16). After ensuring the homogeneity of the alginate solutions under a phase contrast microscope, we were able to proceed with using the microfluidic devices.

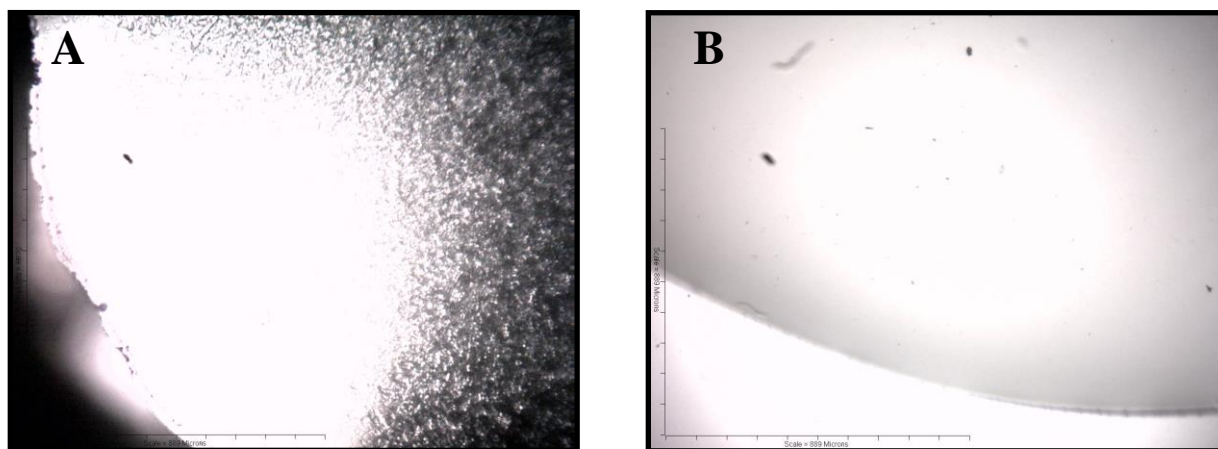


Figure 16: The Importance of Using a Magnetic Stirrer when Preparing Alginate Solutions
(a) A drop of 2% alginate solution *without* the use of a magnetic stirrer. Large particles of undissolved alginate is conspicuous. (b) A drop of 2% alginate solution *with* the use of a magnetic stirrer. The alginate solution is homogeneous and completely transparent – indicating the purity of the solution.

Testing the Microfluidic Devices

Before we tested the cross-linking reaction of sodium alginate and CaCl_2 in the microfluidic device, we used water to observe the flow of liquid through the channels. Green food coloring was used in the water to make the expected flow of CaCl_2 in the outer two inlet channels more apparent. The middle channel, which was designated for alginate, was replaced with clear water for the same purpose (Figure 17).

After ensuring that liquid was flowing through the device properly, we progressed to use CaCl_2 and sodium alginate. We found that the most ideal rate for the two outer CaCl_2 channels had CaCl_2 flowing five to ten times faster than the middle alginate channel. Doing so allowed the alginate to be compressed by the CaCl_2 from both sides; thus yielding smaller alginate microfibers. Some of the channels became clogged with calcium-alginate because the alginate and CaCl_2 were not pumped in at controlled rates (Figure 18). To assist in the unclogging of the channels, the microfluidic devices were soaked in sodium citrate overnight.

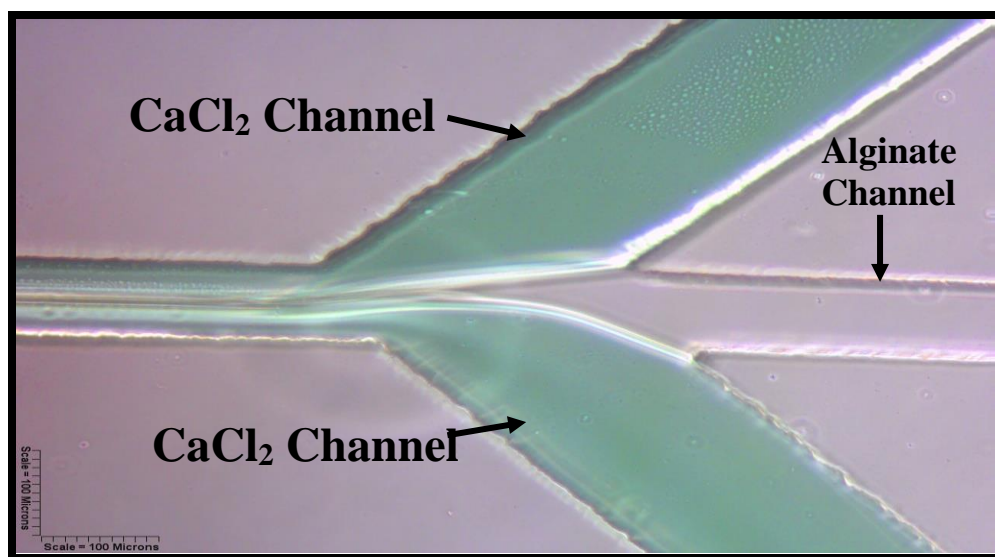


Figure 17: Test of a Functional Microfluidic Device

Green food coloring with H_2O was used in place of CaCl_2 in the outer two inlet channels. H_2O without food coloring was used to demonstrate the expected flow of alginate in the middle channel.

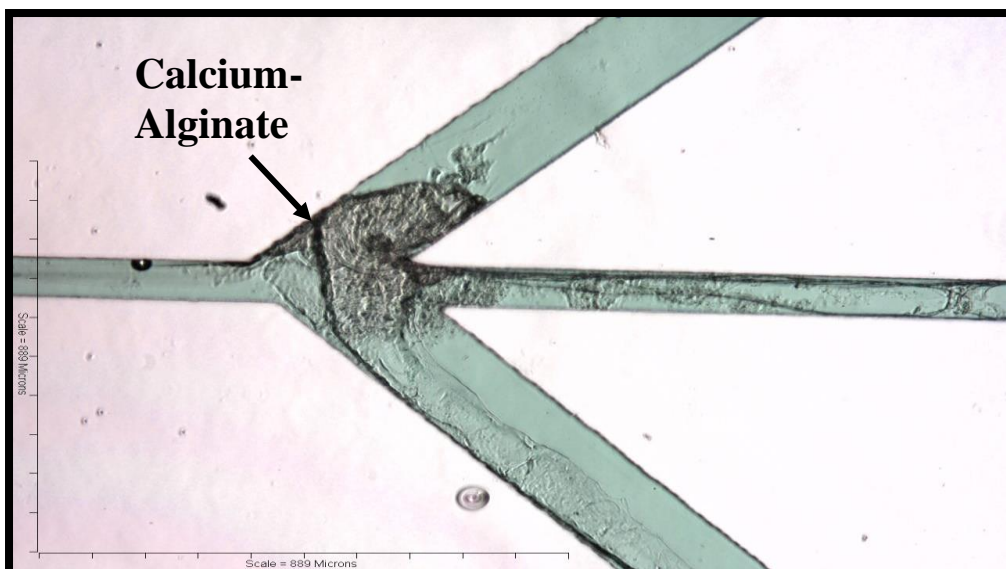


Figure 18: A Microfluidic Device Clogged with Calcium-Alginate
Calcium alginate is apparent at the junction of this three-way device. The clogging occurred due to inconsistent pumping of the solutions

Cell Encapsulation via Passive Flow through SU8 Filters

Various concentrations of alginate containing mESCs were dropped onto each of the twelve porous units of the SU8 structure (Figure 19). In most cases, it was difficult for alginate microfibers to form. The solutions either coalesced before forming any alginate fibers, or did not flow through the pore at all (Figure 20). After treatment with 25mM sodium citrate to dissolve any calcium-alginate that may have clogged the pores, the alginate microfibers still did not form. The SU8 passive flow technique was repeated using a new batch of SU8 photoresist filters. After suspending the living cells in sterile alginate, the gel matrix was poured onto the pores. The alginate was then treated with a curing solution of aqueous CaCl_2 . To prevent the alginate fibers from breaking during liquefaction of their interior, 1mL of 0.05% poly-L-lysine hydrobromide (polylysine) in 0.9% NaCl was added to the microfibers (Figure 21).

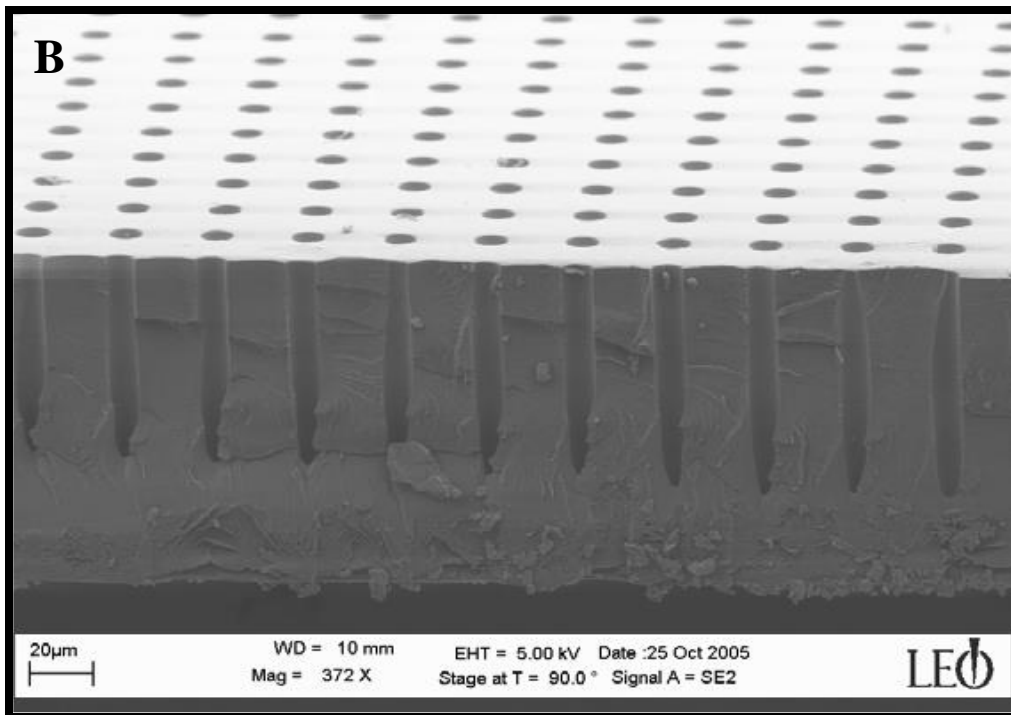
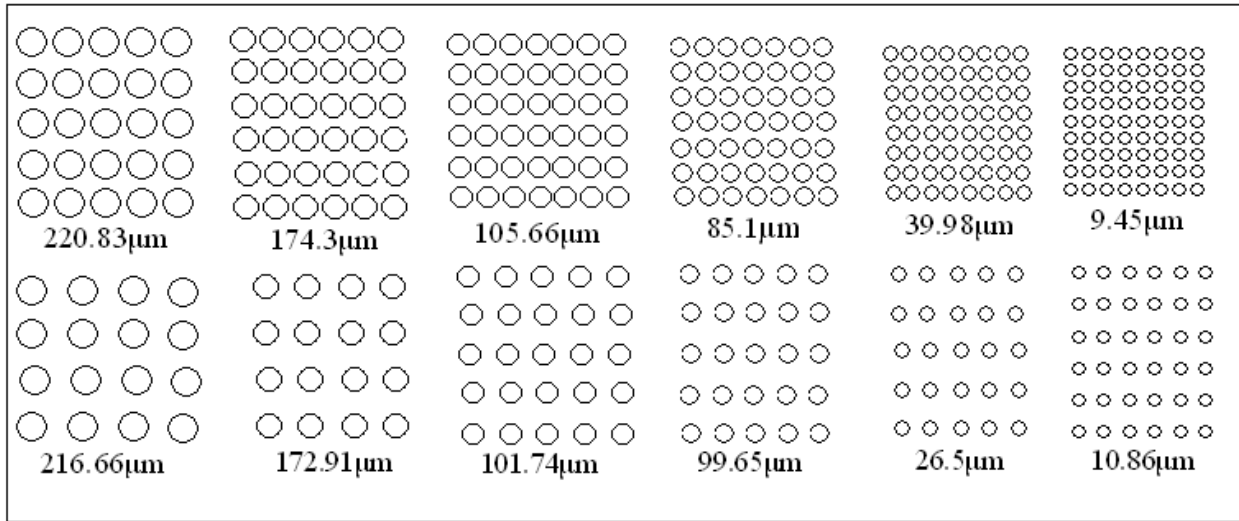
A

Figure 19: SU8 photoresist Filter with Twelve Porous units.

(a) The top row contains condensed pores and the bottom contains non-condensed pores. The average pore sizes of each unit are labeled underneath. (b) SEM (Scanning electron microscope) image of a cross-section through the pores on an SU8 photoresist.

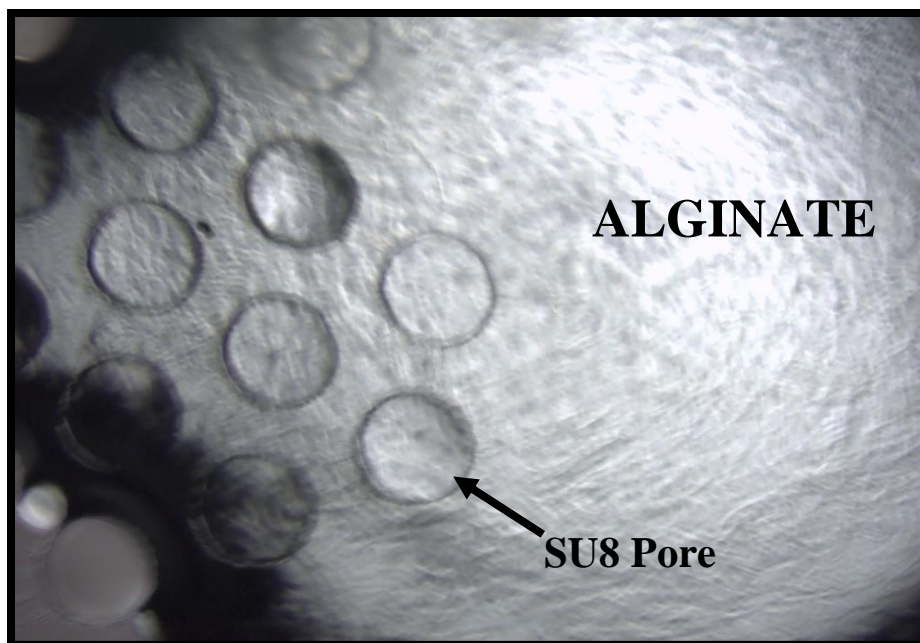


Figure 20: A droplet of Alginate on Pores of an SU8 Filter
 Alginate is unable to pass through the pores due to back flow of CaCl_2 .

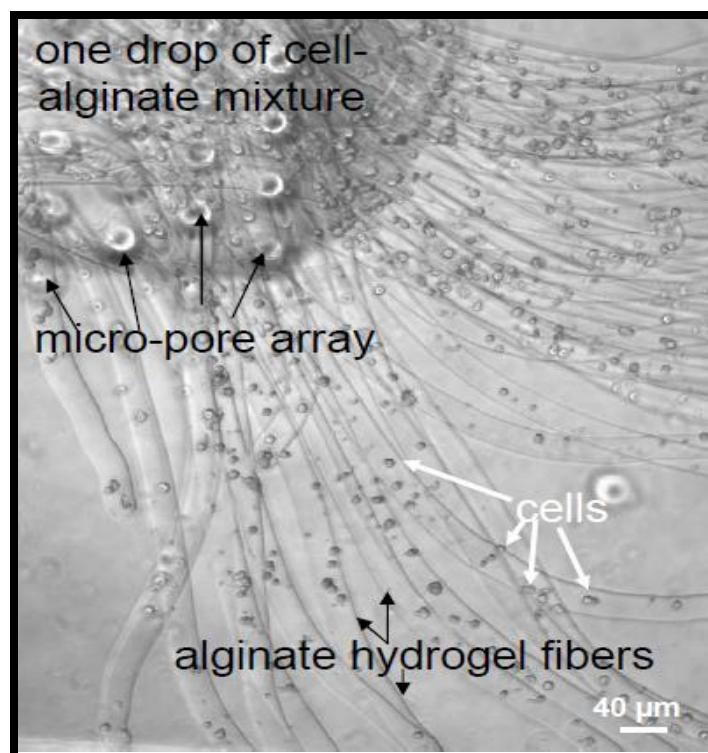


Figure 21: Cells Encapsulated Inside Alginate Hydrogel Microfibers
 A drop of the cell-alginate solution can be seen on top of the filter before cross-linkage with CaCl_2 . The microfibers form upon contact with the curing solution.

Right-Side up Microfluidic Extrusion Device

We discovered that after extruding the alginate through the SU8 device, the alginate would find a pore that it was most comfortable with and form a single microfiber from it (Figure 22). When multiple strands of alginate reached the surface of the filter they tended to coalesce. This occurred because the alginate microfibers were heavier and denser than the aqueous CaCl_2 . As a result, gravity naturally brought them together towards the bottom causing them to clump into one large unit. To surmount this problem, we tried a different approach with the SU8 device upside down and completely submerged in CaCl_2 . However, this approach also posed a slight problem. The alginate fibers would coalesce together in very much the same way they did with the right-side up extrusion device.

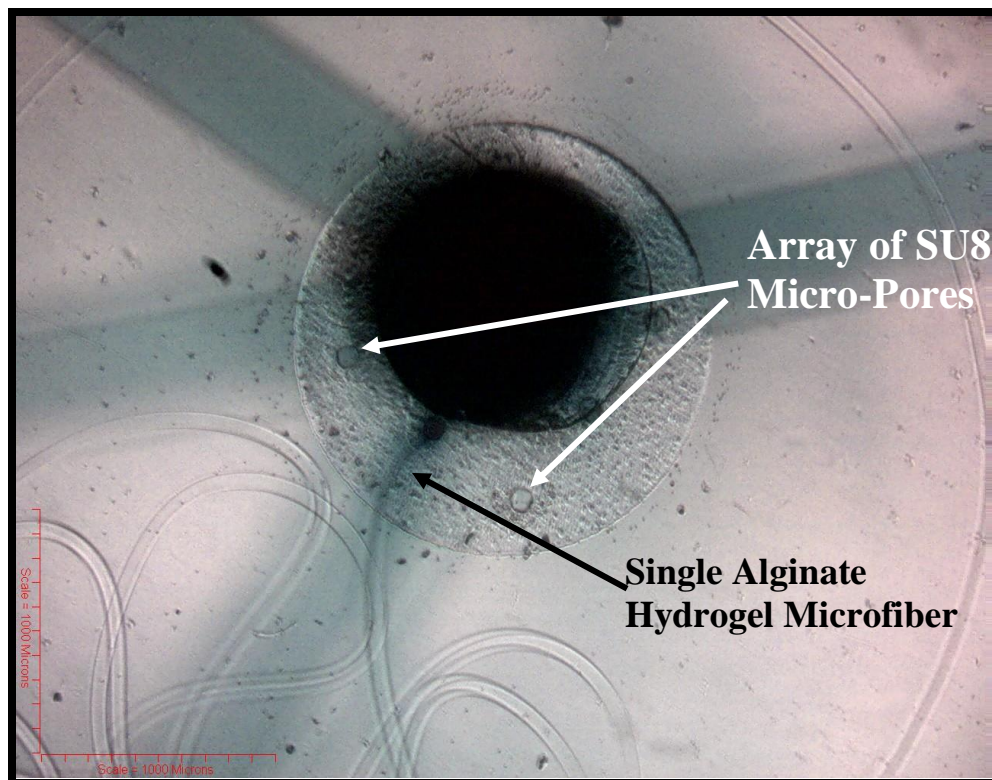


Figure 22: Right-Side up SU8 Microfluidic Extrusion Device
A single alginate hydrogel microfiber is being extruded from the pore it found to be most comfortable.

Microfluidic “Snake Channel” Devices

Syringe pumps were used to control the rates at which the corn oil, alginate, and CaCl_2 flowed into their respective channels. During this process, some back flow was observed because of a poor seal at the point of tube insertion (Figure 23). To correct this problem, we adjusted the flow rates of the corn oil channel and the alginate channel so that they were flowing in a 3:1 ratio at $15\mu\text{L}/\text{min}$ and $5\mu\text{L}/\text{min}$ respectively. For each channel, different flow rates were tested to find the ideal speeds for bead formation (Figure 24a-b).

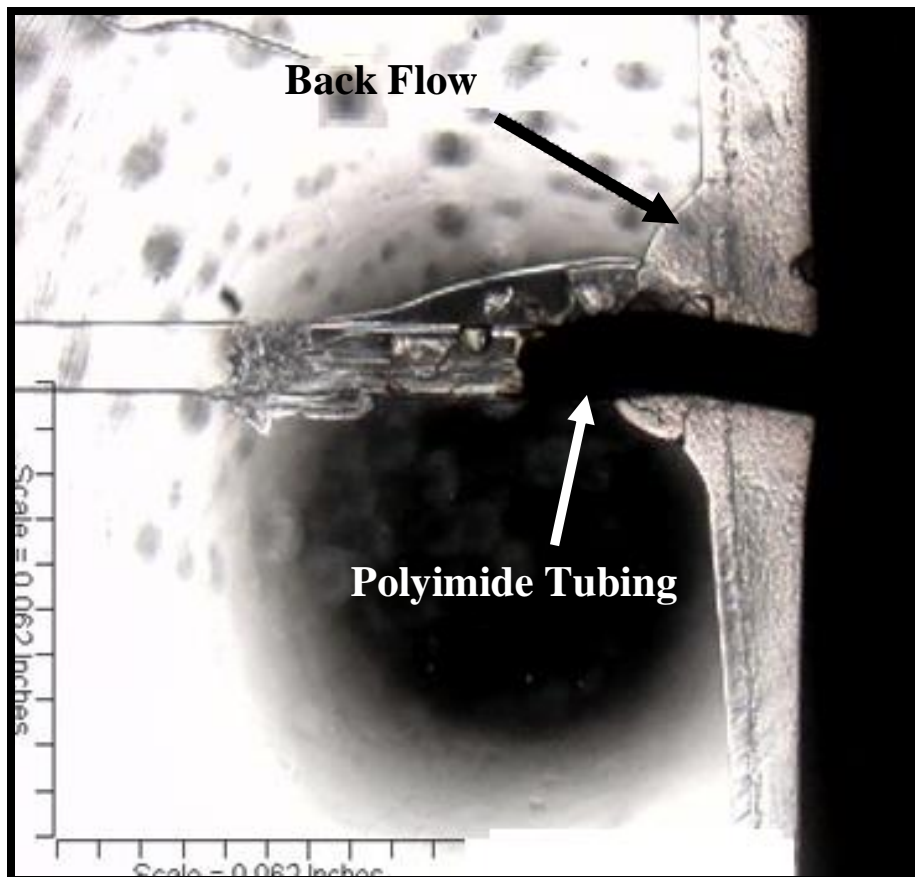


Figure 23: Microfluidic “Snake Channel” Device with Poor Seal
The seal causes leakage and back flow of corn oil channel.

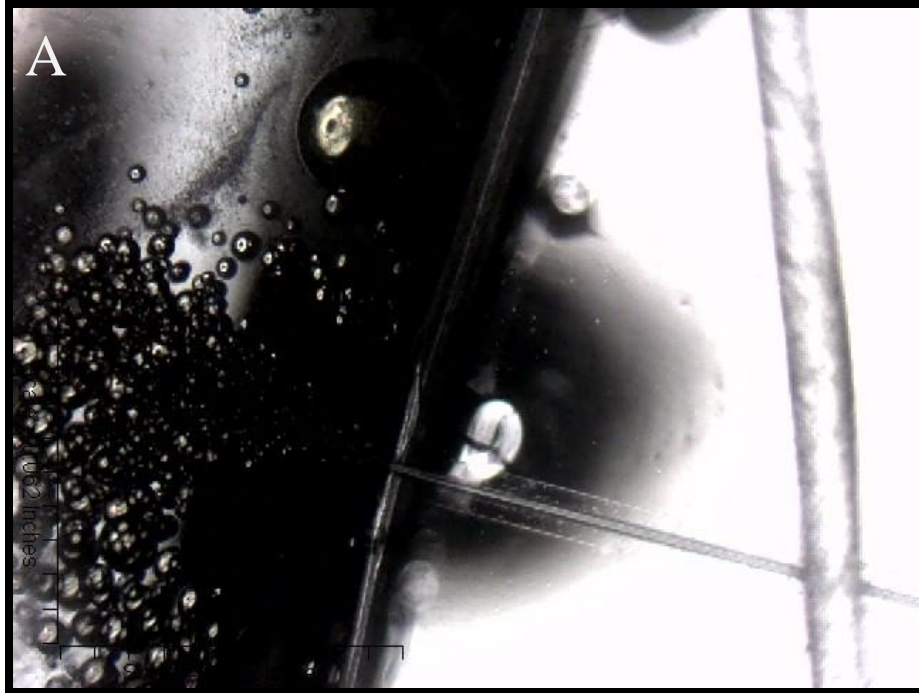


Figure 24: Testing of Flow Rates in the Microfluidic “Snake Channel” Device

(a) Beads coalesce into one unit after exiting from the channel. The clear transparent/yellow fluid surrounding the beads is corn oil. (b) The size of the microbeads can be controlled by changing the rates at which each substance is pumped. Ideal speeds consist of corn oil flowing at $15\mu\text{L}/\text{min}$ and alginate at $5\mu\text{L}/\text{min}$ (3:1).

Discussion

Of the methods that we tested, encapsulating cell via passive flow through SU8 filters was by far the most efficient approach for making alginate microtubes or “noodles”. However, the results were not very consistent. Alginate fibers seldom formed in the aqueous calcium chloride curing solution. The hydrophilic tendencies of calcium chloride would cause the filter pores to become clogged, thereby preventing the sodium alginate from flowing through the filter altogether. To overcome this dilemma, SU8 filters with hydrophobic undersides and hydrophilic pores will have to be made to prevent the uptake of CaCl_2 . The few times that the hydrogel alginate fibers did form, the strands had numerous kinks, which were an indication that the fiber walls were not strong enough (Figure 25). Using multiple layers of polylysine to coat the outside of the fiber could strengthen the hydrogel fiber by building up its thickness. This process would prevent the hydrogel microfiber from breaking.

Active microfluidic approaches were used throughout this project to control the rates at which alginate and calcium chloride were pumped into the microfluidic devices. The device consisting of three inlet channels – one for alginate and two for CaCl_2 – formed alginate microfibers as long as the channels were not clogged with cross-linked alginate or epoxy glue. To prevent calcium-alginate from blocking the channels, it was advisable to use syringe pumps set at controlled rates as opposed to using manual force to pump the solutions.

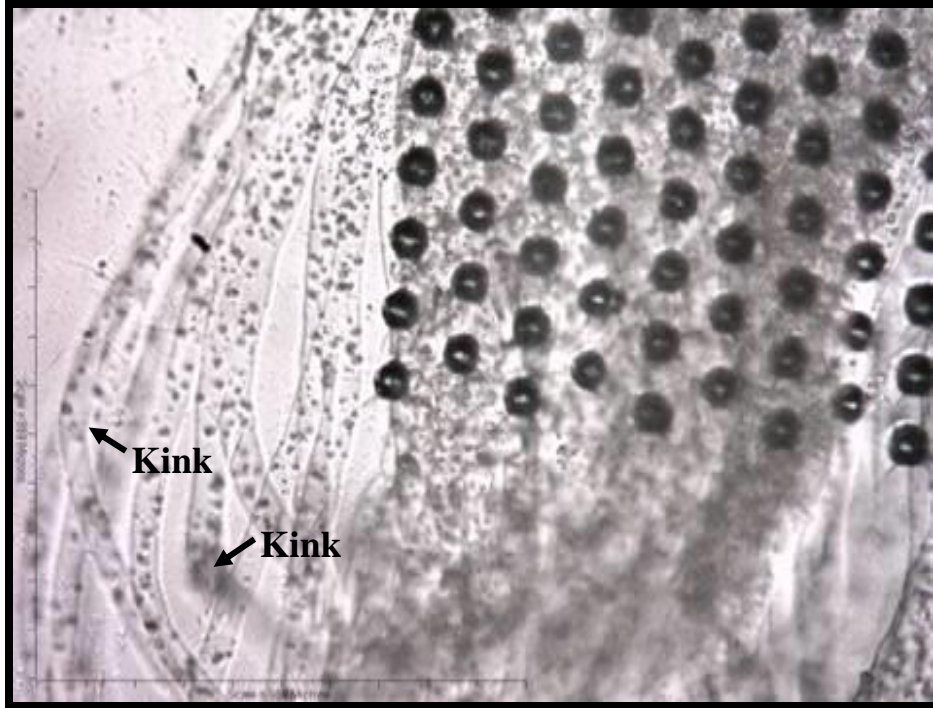


Figure 25: MESCs Encapsulated in Alginate Hydrogel Fibers
The small kinks formed because the fibers were not treated with polylysine.

The SU8 microfluidic extrusion techniques served as appropriate replacements for the passive flow SU8 filters. They both involved applying an external force to pump the sodium alginate solutions directly through the porous structures on the SU8 filter. Using the filters also helped control the diameter of the alginate fibers because each porous structure had a unique size (Figure 26). The only problem that arose while testing the active SU8 technique was that the fibers coalesced as soon as they passed through the filter pores. This made it impossible to generate long hydrogel microfibers. To surmount this problem, we attempted to immerse the microfluidic SU8 device upside down in aqueous CaCl_2 (Figure 11). Although gravity assisted the alginate fibers in forming quicker, they still had a tendency to coalesce into one massive hydrogel unit.

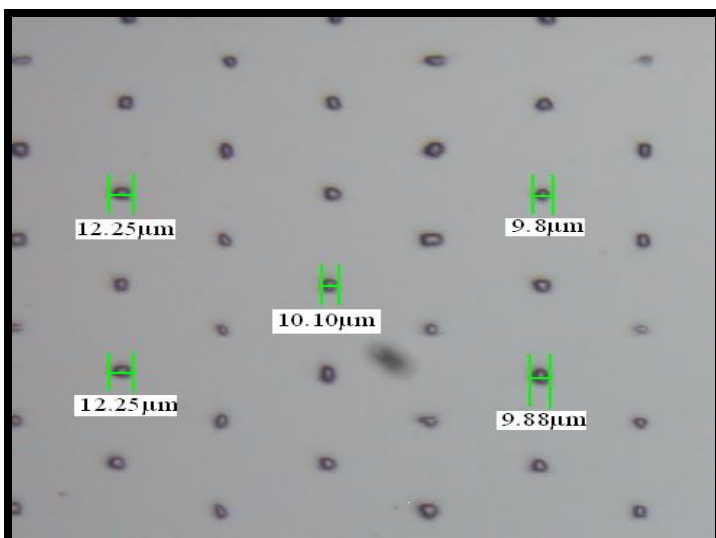


Figure 26: Small Porous Structures on an SU8 Photoresist Filter

This is one out of the twelve porous units embedded on the SU8 filter. The average pore size of this condensed unit is $10.86\mu\text{m}$ ($n = 5$).

The agarose molds, although relatively simple to fabricate, were not very effective in forming hydrogel fibers. One of the main reasons was because when alginate was dropped onto a channel on the agarose mold, there was no way to control its flow rate. The alginate travelled quickly along the hydrophilic surfaces of the channel by capillary action (Figure 27). A long hydrogel fiber formed when the entire assembly was submerged into aqueous calcium chloride. To collect the alginate microfibers, the agarose mold would have to be liquefied again. The only way to go about doing this would be to reheat the agarose substance. This process would obviously be a severe detriment for the viability of the cells inside the alginate solution.

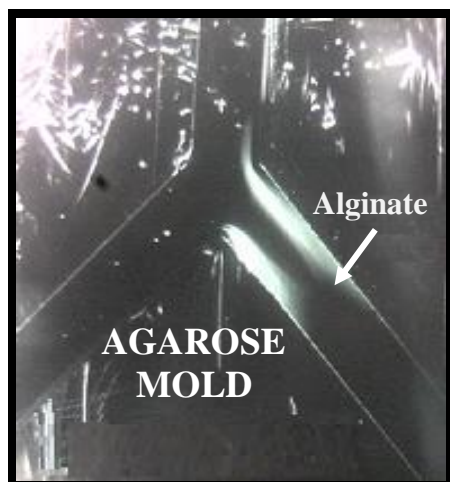


Figure 27: Microfluidic Channel Engraved on an Agarose Gel Mold

2% alginate solution is drawing from the bottom right channel via capillary action. When the entire agarose-alginate assembly is submersed into an aqueous cross-linking solution of CaCl_2 , the alginate retains the shape of the channel, resulting in the formation of an alginate hydrogel microfiber.

For the aforementioned reasons, using the microfluidic techniques discussed above to fabricate 3-D alginate tissue constructs was discontinued. We hypothesized that simpler and more consistent methods could be employed to surmount the problems we observed with the microfluidic devices. By doing so, we were able to seed cells onto biocompatible matrices on a regular basis. In the upcoming chapters that follow, we describe several of those techniques and explain how they were used to overcome the issues that we faced in chapter 1.

Chapter 2:

“Synthesis of 3-D Alginate Nanofibers Using the Electrospinning Technique”

Introduction

Nanofibers have become a commonly used scaffold for cell growth in tissue engineering applications due to their ability to mimic the extracellular matrix naturally found in tissues (Teo, et al., 2006). Electrospinning is a simple method that has proven itself to be highly effective in fabricating ultra-fine 3-D fibers with diameters on the nanoscale. During the process of electrospinning, the resultant nanofibers are randomly deposited, creating a large surface area and highly porous nanofibrous mat. These two conditions predispose the natural architecture and the topography of the *in vivo* biological extracellular matrix to be mimicked (Figure 28) – which, in effect, has great potential for tissue engineering endeavors (Lu, et al., 2006).

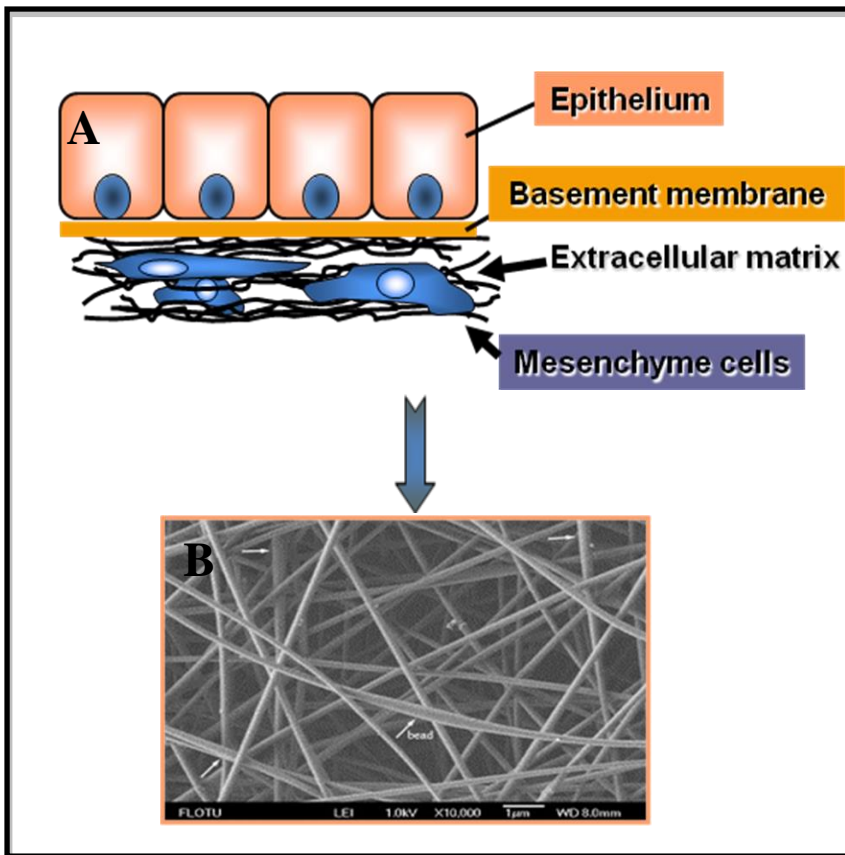


Figure 28: Electrospun Nanofibers Simulate the Biological ECM
(a) *In vivo* representation of the biological ECM
(b) 3-D alginate nanofibers generated through the process of electrospinning can mimic the architecture of the ECM *in vivo* (Lu, et al., 2006)

Alginate, as mentioned previously, is a great biomaterial to use for bioengineering purposes because of the physical properties it possesses. However, alginate is not necessarily ideal to use for Microelectromechanical System (MEMS) applications like electrospinning because of its anionic character caused by the presence of negatively-charged carboxyl groups (Figure 5), and its poor viscoelasticity.

For the reasons emphasized above, pure alginate does not have the ability to undergo electrospinning solitarily. Therefore, to facilitate the process of electrospinning with alginate, the polymer must be blended with a suitable solvent to decrease the conductivity and to enhance the chain entanglements of the molecule. Research suggests that the addition of the solvent functions to interrupt the inter- and intramolecular hydrogen bonds that occur among the alginate chains, and form new hydrogen bonds that are more flexible than the previous (Nie, et al., 2008). We hypothesized that polyethylene oxide (PEO), a biocompatible and non-toxic synthetic polymer, would be able to fulfill these conditions and promote the electrospinning of alginate (Figure 29).

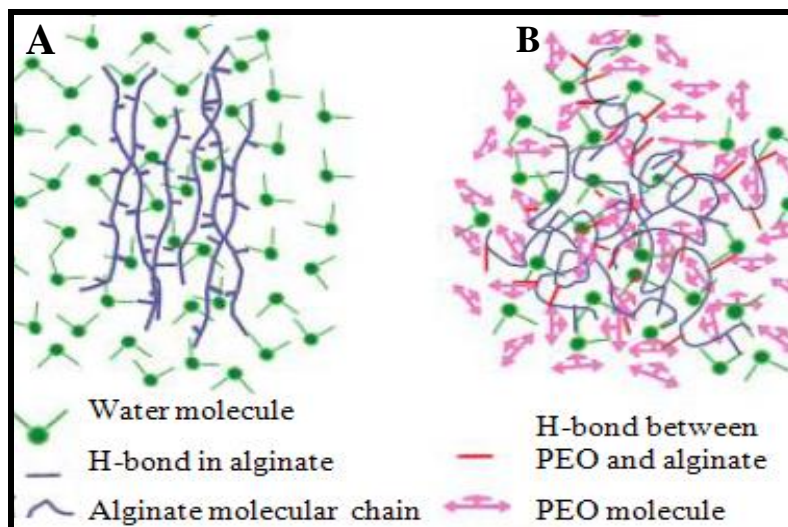


Figure 29: Illustration Depicting Chain Entanglements of Alginate Molecule

(a) When pure alginate is blended solely with water, the aqueous solution is inadequate to produce electrospun nanofibers because of the rigid molecular entanglements present between molecules. (b) PEO enhances the chain entanglements that occur between the molecules by introducing new, flexible hydrogen bonds. (Nie, et al., 2008)

In the experiments that follow, we investigated the effect of altering the alginate/PEO ratios, and changing the overall concentration of the polymer solution. We also sought to optimize nanofiber morphology by electrospinning alginate solutions with two molecular weight versions of PEO – 400 kDa and 900 kDa to produce alginate-based nanofibers on the nanoscale.

Materials and Methods

Preparation of Alginate/PEO Solutions

Preparing aqueous alginate/PEO solutions with ideal viscoelastic properties was an important milestone for the progress of this experiment. We experimented with low viscosity (250 cps) and medium viscosity ($\geq 2,000$ cps) forms of sodium alginate, and 400 kDa and 900 kDa molecular weight versions of PEO. Both polymers were purchased from Sigma-Aldrich (United States), and used in pure forms. Alginate/PEO polymer solutions were prepared in different concentrations and in varying ratios by first dissolving the alginate and PEO in distilled water (Table II). The mixtures were then magnetically stirred overnight at room temperature to obtain homogeneous solutions.

Assembly of the Electrospinning Apparatus and Synthesis of 3-D Alginate Nanofibers

Our innovative electrospinning technique involved applying a high external voltage power supply, typically between 10kV and 20kV, to the polymer solution of alginate and PEO contained in a syringe. The continuous charge induced an electrical current within the fluid. Once the charges in the solution breached a critical threshold point, a polymer jet, referred to as a Taylor Cone, erupted from the solution droplet at the tip of the syringe needle (Taylor, 1964). The excessive charge repulsion that occurred at the syringe needle tip led to the ejection of the

alginate/PEO solution. Since current has a propensity to flow from high potential energy to low potential energy, the solution streamed down toward an oppositely charged grounded collector plate of lower potential energy. As the polymer jet accelerated toward the grounded collector plate, the PEO solvent in the solution evaporated – leaving behind a porous mat of dry, solidified alginate nanofibers (Figure 30).

Table II: Preparation Protocol for Alginate/PEO Solutions

Solution	Sodium alginate /PEO Ratio	Concentration (%) $\frac{\text{solute}}{\text{solute} + \text{solvent}}$	Alginate Viscosity (cps)	PEO MW (kDa)
1	1:1	2 %	250 cp	400 kDa
2	1:1	3%	250 cp	400 kDa
3	1:1	4%	250 cp	400 kDa
4	1:1	5%	250 cp	400 kDa
5	1:1	2%	$\geq 2,000$ cp	400 kDa
6	1:1	3%	$\geq 2,000$ cp	400 kDa
7	1:1	4%	$\geq 2,000$ cp	400 kDa
8	1:2	2%	250 cp	400 kDa
9	1:2	3%	250 cp	400 kDa
10	1:2	4%	250 cp	400 kDa
11	1:2	2%	250 cp	900 kDa
12	1:2	3%	250 cp	900 kDa
13	1:2	4%	250 cp	900 kDa

Solutions were prepared in varying ratios of alginate/PEO (1:1 and 1:2), different overall concentrations ranging from 2% to 4%, two molecular weight versions of PEO (400 kDa and 900 kDa), and two viscosities of alginate (250 cp and $\geq 2,000$ cp).

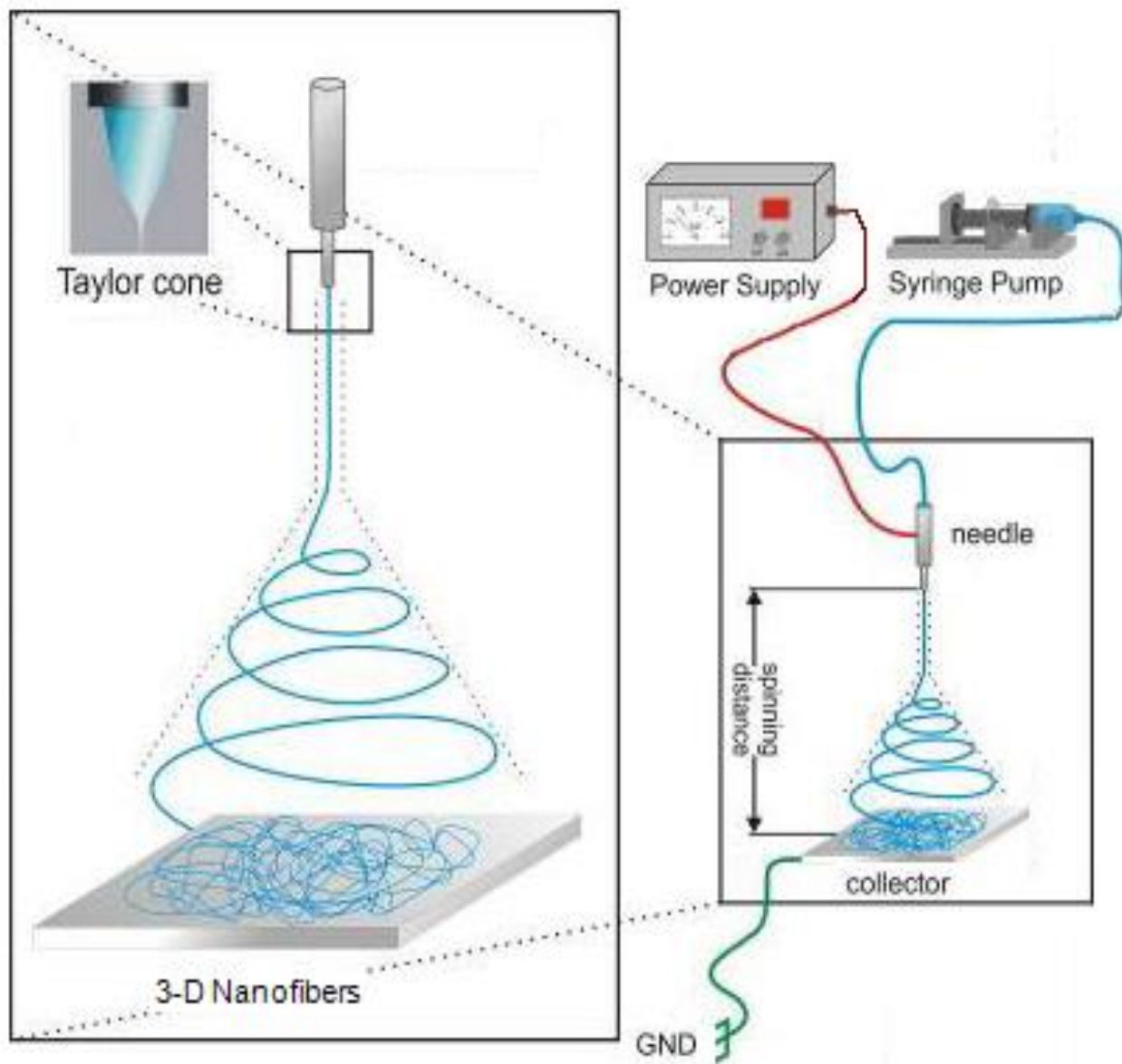


Figure 30: Assembly of the Electrospinning Apparatus

The apparatus consists of an external DC voltage power supply (10-20 kV). The spinning distance from the tip of the syringe needle to the grounded collector plate was set between 10cm and 15 cm depending on the viscosity of the solution. Pump speeds were set to rates in the $\mu\text{L}/\text{min}$ range (George, 2009).

Results

Effect of the Concentration of the Overall Solution

After assembling the electrospinning apparatus as shown in figure 30, the alginate nanofibers were synthesized using polymer solutions that differed in several parameters. The overall trend we observed was that as the concentration of the polymer solution increased gradually, the general shape of the nanofibers changed from being spherical to spindle-like, until they finally obtained a smooth appearance (Figure 31a-c). The alginate/PEO solution that yielded nanofibers with optimal morphology was that of 4%, our highest overall concentration solution.

Effect of the Ratio of Alginate to PEO in Solution

To investigate whether nanofiber morphology was dependent on the proportion of alginate in solution with PEO, we prepared alginate/PEO solutions of different ratios. After electrospinning the solution with equal amounts of alginate and PEO, we observed heavy beading, or spherical structures in the nanofibrous mat. This was an indication that the solution being electrospun did not have the viscoelastic properties conducive to producing smooth fibers (Figure 31a). The smoothest nanofibers were produced with the solution consisting of a low proportion of alginate (1:2 – 1 parts alginate to 2 parts PEO) as shown in Figure 31c. However the solutions consisting of a 1:2 ratio of alginate/PEO and a 400 kDa molecular weight PEO did not produce smooth nanofibers. This observation suggested that the molecular weight of PEO might play a role in the performance of electrospinning as well.

Effect of the Molecular Weight of PEO

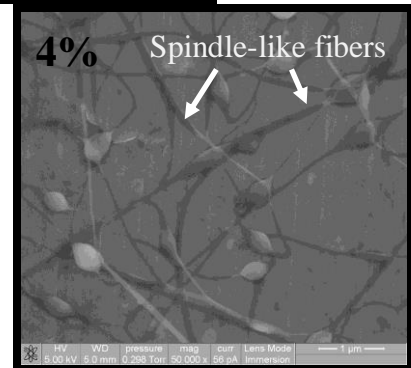
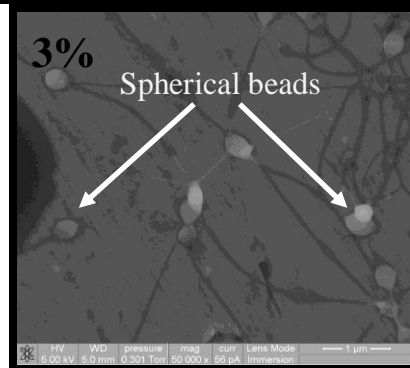
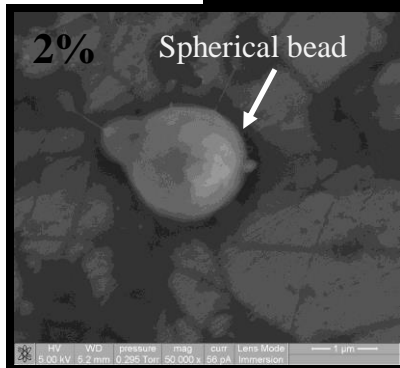
We examined the effect of increasing the molecular weight of PEO in solution from 400 kDa to 900 kDa (Figure 31d). Comparing the morphology of the electrospun nanofibers in figure 31b to those in figure 31c provided evidence suggesting that the molecular weight of PEO was important in facilitating effective electrospinning. As we changed the molecular weight of PEO from 400 kDa to 900 kDa in the 4% solution with a 1:2 ratio of alginate/PEO, we observed an overall improvement in the morphology of the nanofibers. Increasing the molecular weight of the PEO solvent allowed the nanofibers to adapt a smoother appearance without the beads being too apparent. Beading was considered a hindrance for the process because cells are not able to seed effectively to the scaffolds when there is a preponderance of beads.

Effect of Viscosity on the Process of Electrospinning

We found that there was a direct connection between the parameters discussed above (solution concentration, alginate/PEO ratio, and PEO molecular weight) and the viscosity of the polymer solution. Using a viscometer, we obtained viscosity data for each of our polymer solutions (Fig. 31). These data cohered with our hypothesis that the higher the viscosity, the more enhanced the chain entanglements between the polymers in solution should become. This phenomenon, in turn, had a strong effect on improving the mechanical stability and morphology of the electrospun alginate nanofibers.

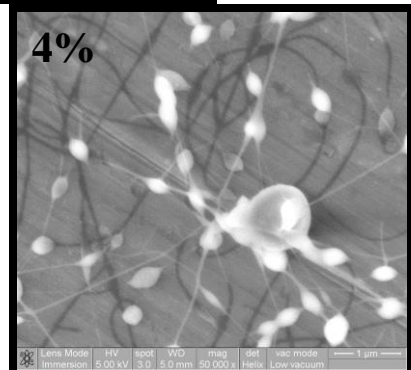
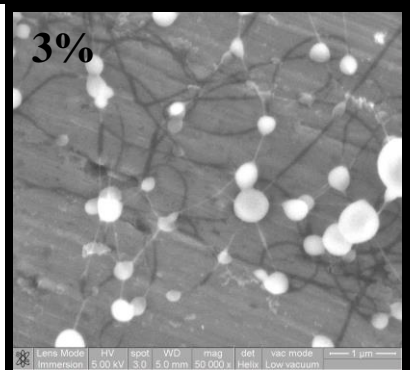
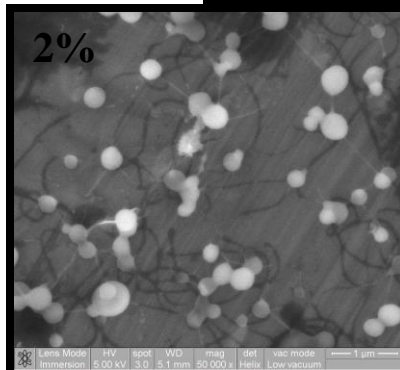
(A)

Alginate and 400kDa PEO in a 1:1 Ratio			
<i>Overall Wt %</i>	<i>Alginate (g)</i>	<i>PEO (g) 400kDa</i>	<i>Viscosity (cP)</i>
2.0%	0.105	0.105	521
3.0%	0.153	0.153	936
4.0%	0.21	0.21	1859



(B)

Alginate and 400kDa PEO in a 1:2 Ratio			
<i>Overall Wt %</i>	<i>Alginate (g)</i>	<i>PEO (g) 400kDa</i>	<i>Viscosity (cP)</i>
2.0%	0.051	0.102	129
3.0%	0.11	0.22	1862
4.0%	0.153	0.306	2358



(C)

Alginate and 900kDa PEO in a 1:2 Ratio			
<i>Overall Wt %</i>	<i>Alginate (g)</i>	<i>PEO (g) 400kDa</i>	<i>Viscosity (cP)</i>
2.0%	0.051	0.102	80
3.0%	0.11	0.22	5795
4.0%	0.153	0.306	5957

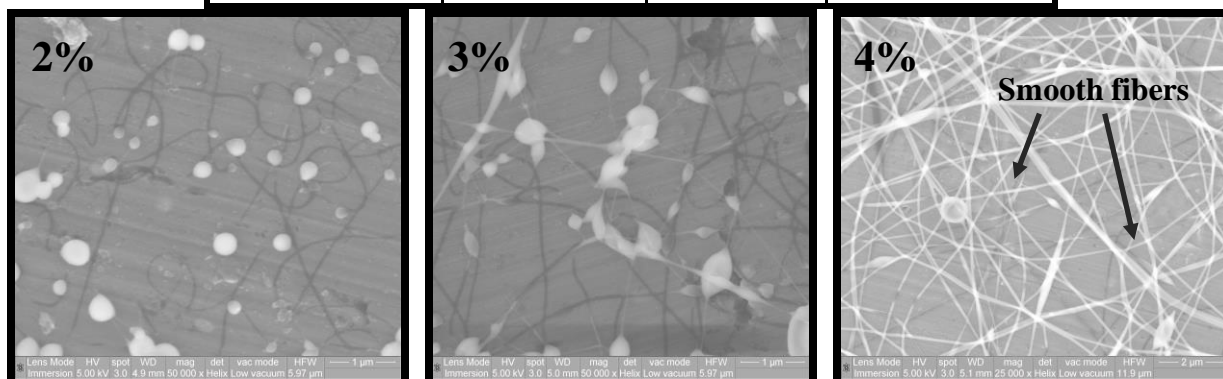


Figure 31: SEM Images of 3-D Alginate Nanofibers of 2%, 3%, and 4% Concentrations

(a) Nanofibers consisting of alginate and 400 kDa PEO [1:1] (b) Nanofibers consisting of alginate and 400 kDa PEO [1:2] (c) Nanofibers consisting of alginate and 900 kDa PEO [1:2]

Discussion

The length of any polymer chain is generally representative of its molecular weight. Due to this fact, we investigated nanofiber morphology with 400 kDa and 900 kDa molecular weight versions of PEO. By increasing the molecular weight of the PEO solvent, it was possible to increase the degree of chain entanglements occurring within the solution. This minor parameter adjustment ultimately had a direct effect on the solution viscosity, which in turn improved the morphology of our electrospun nanofibers so that they could best resemble the biological ECM.

Viscosity, as suggested above, plays a vital role in the overall performance of electrospinning. However, it has to be maintained within a specific threshold, otherwise

electrospinning will not be effective in producing nanofiber scaffolds. We were able to suggest that a minimum level of viscosity must be achieved within the alginate/PEO polymer solution to facilitate the process. To optimize this level, we experimented by changing the molecular weight of PEO, the overall concentration of the solution, and the ratio of alginate to PEO in aqueous solution. However, it was imperative to ensure that the viscosity did not surpass a certain point at which the solution would become too difficult to pass through the syringe needle tip (Kameoka, et al., 2003). Furthermore, a solution of too high viscosity would have caused the fluid to dry up and solidify at the tip of the syringe needle prior to the initiation of electrospinning (Zhong, et al., 2002). Based on these factors, we were able to conclude that the viscosity of the solution was a critical component in the performance of electrospinning as well as in the morphology of the nanofibers.

This electrospinning method used to produce nanofibers out of alginate may be useful in the future for engineering an artificial salivary gland. However, this technique will obviously require further optimization since we were not able to generate smooth nanofiber matrices without beading being present. Nevertheless, a major advantage of using alginate for the production of nanofibrous scaffolds is that the resulting nanofibers have low stiffness values; which, in effect can mimic the actual stiffness of natural biological tissue better than other artificial biomaterials that are commonly used for the synthesis of nanofibers (e.g. PLLA, PLGA). Therefore, we must employ other methods to measure the stiffness of these alginate nanofibers. Then, future studies will investigate the ability of the alginate nanofibers to form scaffolds for salivary cell attachment.

Chapter 3:

“Fabrication of 3-D Alginate Microbeads Using the Electrodroplet Technique”

Introduction

The experiments that follow in this chapter demonstrate the use of the electrodroplet technique to fabricate 3-D alginate hydrogel microbeads for *in vitro* cell cultivation. The shape of the alginate beads may mimic the structure of acini present *in vivo*. It is well known that in order for cells to grow properly, they must be anchored onto a surface, thus facilitating their proliferation. However, as it was mentioned before, cell adhesion to alginate microbeads is not ideal, as has been demonstrated in other studies (Hou, et al., 2005). Therefore, the membrane of the microbead must be modified by applying additional surface coatings to induce attachment. Cells do not attach to alginate effectively because cell walls are typically negatively charged. The alginate molecule contains negatively charged carboxyl groups. Thus, the anionic characters expressed by both the cells and the alginate microbeads contribute to their inability to attach to one other. To solve this problem, we hypothesized that gelatin, fetal bovine serum (FBS), poly-L-lysine (PLL), and fibronectin would be effective surface coats in promoting cell adhesion to the alginate microbeads.

Gelatin is a protein extracted from the skin, bones, and connective tissues of animals. It is an irreversible hydrolyzed derivative of collagen. When gelatin is exposed to heat, it attains fluid-like properties. However, when it is cooled, it has a propensity to turn into a hydrogel substance. This solidified form is beneficial for a variety of biomedical applications, including tissue engineering, pharmaceuticals, and wound healing (Akane, et al., 2005). Gelatin, in its gelled form, has been shown to induce cell adhesion when used as a substrate (Choi, et al., 2004). In fact, it is often used to coat the bottom of glass and polystyrene containers during cell

culture.

FBS was also used to modify the surfaces of our alginate microbeads because it too has been successful in optimizing cell adhesion (Hayman, et al., 1985). FBS is extracted from the blood of bovine fetuses, and is typically used for cell culture purposes due to its high prevalence of growth factors. Research suggests that its adhesion promoting properties can be directly linked to the presence of fibronectin, and other adhesive proteins similar to it.

We hypothesized that fibronectin, an extracellular matrix protein present in all vertebrates, would be a good candidate for coating our alginate microbeads. One of its specific roles is to help provide anchorage for cells in the biological ECM. It contains a series of functionally distinct domains that bind to various heterodimeric transmembrane cell surface receptors, known as integrins, through its cell binding domain that is recognized by the integrins (Figure 32). We hypothesized, that these properties would render fibronectin useful for facilitating cell attachment to our microbeads.

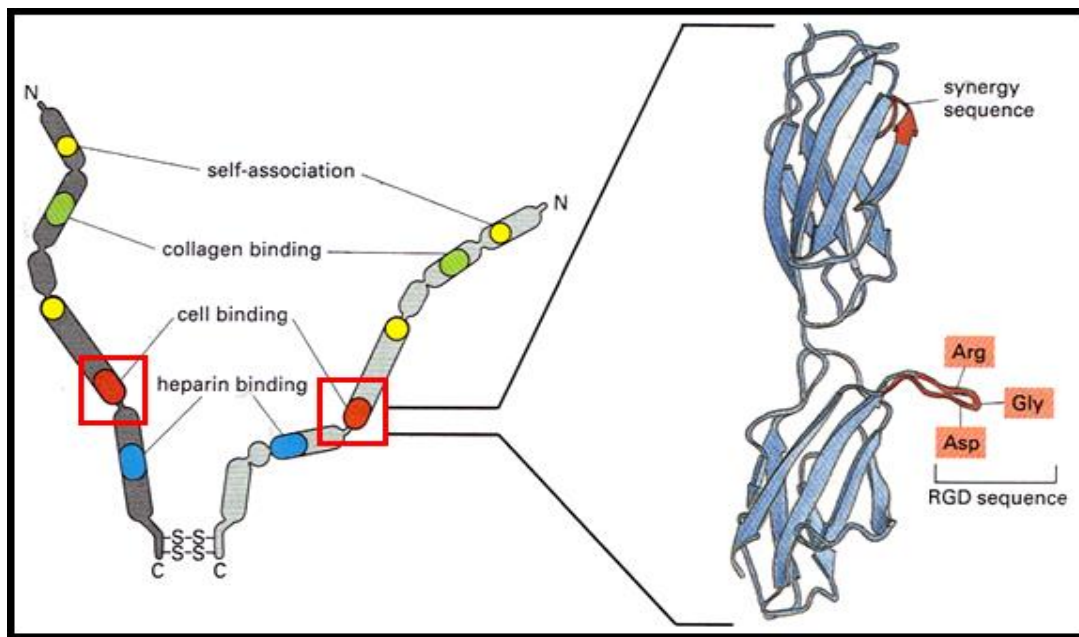


Figure 32: Structure of Fibronectin, an ECM Protein

Fibronectin functions as a ligand for integrin transmembrane receptors in that it helps cells bind to the ECM via its cell binding domain, which forms a binding site for integrins.

Research conducted by Atashi et al. (2009) demonstrated that PLL-coated plastic surfaces had an adhesive effect on cartilage chondroprogenitor cells. This observation coincided with our hypothesis that PLL could promote cell attachment to the microbeads because of the positively charged amine groups present in its molecular structure (Figure 33). We also experimented by designing a multilayer surface coat of alginate, polylysine, gelatin, and fetal bovine to observe any differences in cell attachment in comparison to a single-layer surface coat.

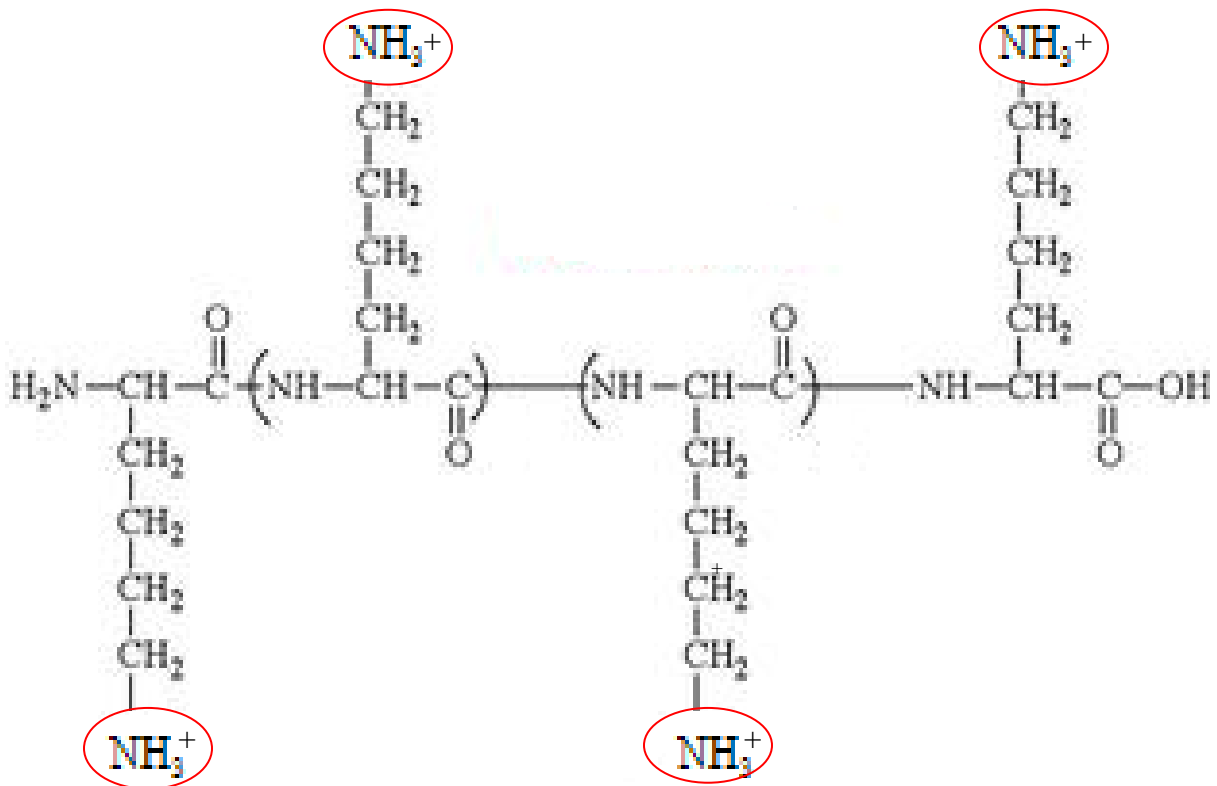


Figure 33: Chemical Structure of the Poly-L-lysine (PLL) Molecule

When protonated, the primary amine groups in the PLL molecule attain a positive charge. This resultant charge promotes cell adhesion because it can attract to the negative charge exhibited by the cell wall. (Lee et al., 2008).

To investigate cell adhesion to the alginate microbeads, we used mouse Embryonic Stem Cells (mESCs), NIH 3T3 fibroblast Cells, and a mouse submandibular gland (SMG) ductal epithelial cell line called SIMS. We started with mESCs as our first cell line because research has discovered their ability to differentiate into desired cell types depending on the components of their microenvironment (Ning, et al., 2010). This observed phenomenon is useful for future studies involving the differentiation of mESCs into salivary gland stromal cells for tissue engineering purposes. NIH 3T3 fibroblast cells, named such because of the way in which their established cell line was discovered (Todaro, et al., 1963), were used secondarily because they are a commonly used cell line that is responsive to fibronectin for adherence. Finally, for conspicuous reasons related to the basis of my project, cell adhesion to alginate microbeads was investigated using the SIMS cell line. We discovered that this preliminary alginate tissue construct was capable of mimicking the characteristics of the salivary gland acinar structure of columnar cells naturally found *in vivo* (Figure 34).

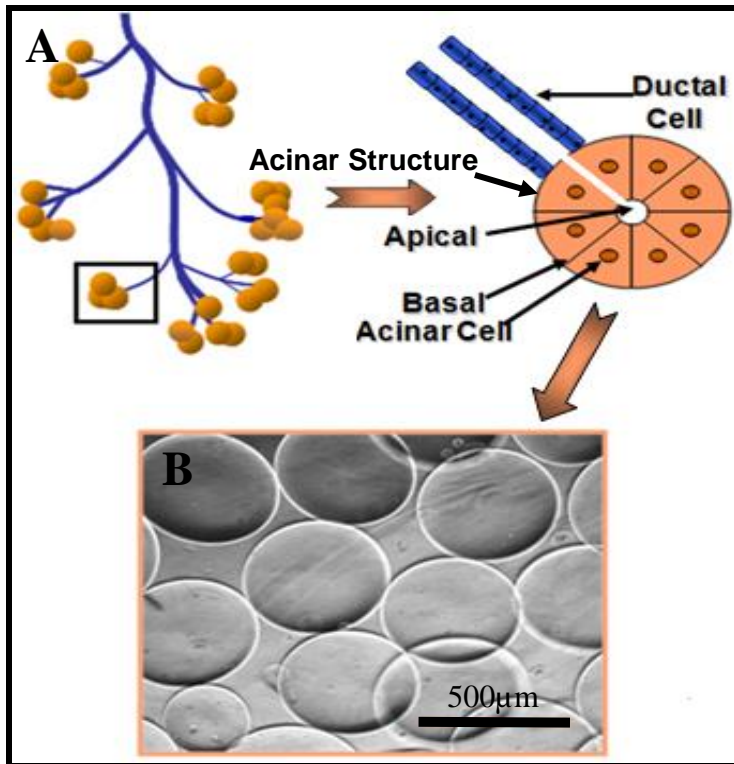


Figure 34: Alginate Microbeads can Simulate Acinar Structure of SG found *in vivo*

(a) *In vivo* depiction of a salivary gland (b) Alginate microbeads fabricated via the electrodroplet technique can emulate the acinar structures.

Materials and Methods

Preparation of Sodium Alginate Solution

Previous experiments performed by Xie, et al. suggested that a 1.5% overall solution concentration of sodium alginate is ideal to use for microbead fabrication purposes. NaCl, is capable of maintaining the ionic strength of the alginate molecule so that it does not lose the integrity of its physical properties during manipulation. Therefore, a 0.9% solution of NaCl (Sigma-Aldrich, United States) was prepared using distilled water. The 0.9% NaCl solution was then used to dissolve the alginate powder (Sigma-Aldrich, United States) and bring it to a 1.5% final concentration. Prior to using the sodium alginate, the mixture was magnetically stirred overnight to obtain a homogeneous solution.

Assembly of Electrodroplet Apparatus and the Synthesis of 3-D Alginate Microbeads

To generate the calcium-alginate microbeads, a modified electrospinning set up was used (Figure 35). The microbeads beads were prepared using a 1.5ml/min syringe pump speed and a ground distance varying between 10cm and 15cm. When the aqueous sodium alginate solution was pumped to the tip of a sterile syringe needle, it was confronted with a charge from the power supply, between 5kV and 10kV. As the voltage, distance to the CaCl₂ curing solution, and flow rate varied, the size and shape of the alginate microbeads varied as well. Typically, spherical microbeads of 10 μ m to 500 μ m in diameter are ideal. When the alginate microbeads came into contact with CaCl₂, they attained an irreversible hydrogel form as a result of the cross-linking reaction that occurred between the two molecules.

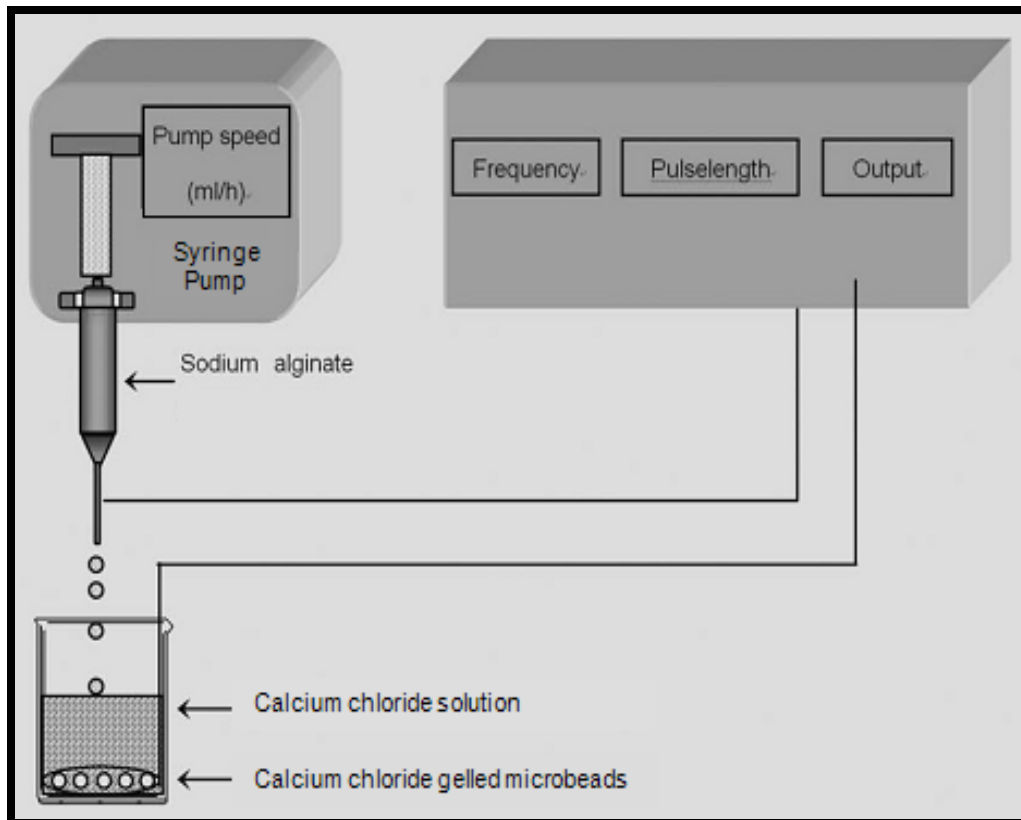


Figure 35: Assembly of the Electrodroplet Apparatus

The electrodroplet technique is similar to the process of electrospinning described in Figure 30. However, the distance from the tip of the needle to the collector is shorter, and the pump rate is slightly faster. The microbeads are also cured in a solution of CaCl₂ following ejection from the needle (Wang, et al., 2006).

Application of Outer Surface Coatings

For the reasons discussed in the beginning of this chapter, cell adhesion to the alginate microbeads without additional surface coatings is not effective. We therefore optimized cell adhesion to alginate by applying gelatin, fetal bovine serum, polylysine, and fibronectin to the outer membrane of the alginate microbeads. We began by washing the beads three times with Phosphate Buffered Saline (PBS) to remove any residual CaCl_2 solution. We then applied a coat of 0.01% or 0.1% gelatin by incubating the alginate microbeads in the gelatin solutions for one hour at room temperature. We repeated this same protocol for the other surface coatings of 100% fetal bovine serum, 0.05% of polylysine, and fibronectin. We also hypothesized that applying successive coats of 0.05% polylysine and 0.15% alginate in between the 1.5% alginate microbead and outer surface coat would optimize cell adhesion (Figure 36). To go about doing this, we incubated each coat for 5-10 minutes at room temperature (Table III).

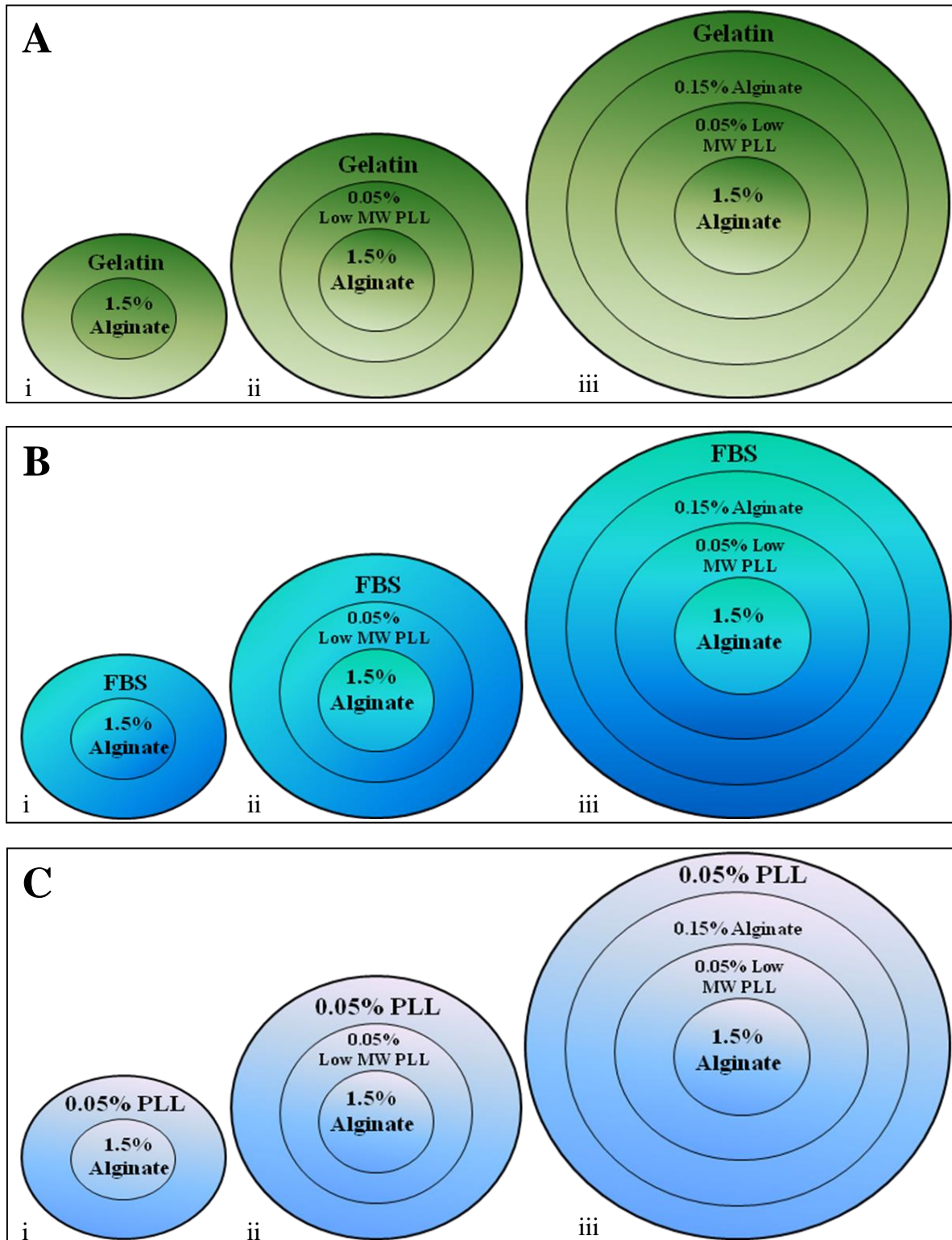

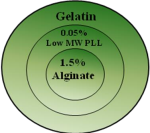
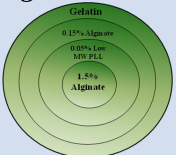
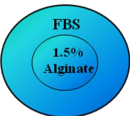
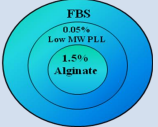
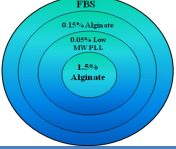
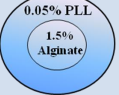
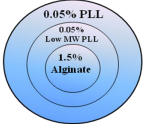
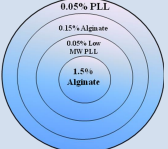


Figure 36: Illustration of Gelatin, FBS, and PLL Multilayer Surface Coats
 (a) Microbeads with multilayers of gelatin [i], PLL-gelatin [ii], & PLL-alginate-gelatin [iii]
 (b) Microbeads with multilayers of FBS [i], low MW PLL-FBS [ii], & low MW PLL-alginate-FBS [iii].
 (c) Microbeads with multilayers of PLL [i], low MW PLL-PLL [ii], & low MW PLL-alginate-PLL [iii].

Table III: Protocol for Applying Multilayer Surface Coatings to Alginate Microbeads

Type of Outer Surface Coat	Procedure
<p style="text-align: center;"><i>Gelatin</i></p> 	<ul style="list-style-type: none"> • Incubate 1.5% alginate microbeads with gelatin for 1 hour at room temperature (R.T.)
<p style="text-align: center;"><i>Gelatin – 0.05% Low MW PLL</i></p> 	<ul style="list-style-type: none"> • Incubate 1.5% alginate microbeads with low MW PLL for 5-10 min. at R.T. • Incubate with gelatin for 1 hour at R.T.
<p style="text-align: center;"><i>Gelatin – 0.15% Alginate – 0.05% Low MW PLL</i></p> 	<ul style="list-style-type: none"> • Incubate 1.5% alginate microbeads with 0.05% low MW PLL for 5-10 min. at R.T. • Incubate with 0.15% alginate for 5-10 min at R.T. • Incubate with gelatin for 1 hour at R.T.
<p style="text-align: center;"><i>Fetal Bovine Serum (FBS)</i></p> 	<ul style="list-style-type: none"> • Incubate 1.5% alginate microbeads with FBS for 1 hour at R.T.
<p style="text-align: center;"><i>FBS – 0.05% Low MW PLL</i></p> 	<ul style="list-style-type: none"> • Incubate 1.5% alginate microbeads with 0.05% low MW PLL for 5-10 min. at R.T. • Incubate with FBS for 1 hour at R.T.
<p style="text-align: center;"><i>FBS – 0.15% Alginate – 0.05% Low MW PLL</i></p> 	<ul style="list-style-type: none"> • Incubate 1.5% alginate microbeads with 0.05% low MW PLL for 5-10 min. at R.T. • Incubate with 0.15% alginate for 5-10 min. at R.T. • Incubate with FBS for 1 hour at R.T.
<p style="text-align: center;"><i>0.05% Polylysine (PLL)</i></p> 	<ul style="list-style-type: none"> • Incubate 1.5% alginate microbeads with 0.05% PLL for 1 hour at R.T.
<p style="text-align: center;"><i>0.05% PLL – 0.05% Low MW PLL</i></p> 	<ul style="list-style-type: none"> • Incubate 1.5% alginate microbeads with 0.05% Low MW PLL for 5-10 min. at R.T. • Incubate with 0.05% PLL at R.T. for 1 hour
<p style="text-align: center;"><i>0.05% PLL – 0.15% Alginate – 0.05% Low MW</i></p> 	<ul style="list-style-type: none"> • Incubate 1.5% alginate microbeads with 0.05% Low MW PLL for 5-10 min. at R.T. • Incubate with 0.15% alginate for 5-10 min. at R.T. • Incubate with 0.05% PLL for 1 hour. at R.T.

Cell Passaging

We thawed trypsin-EDTA, HBSS/PBS (GIBCO), and media in a 37°C water bath until the frozen material disappeared from the trypsin, and the other materials were warmed to 37°C. Each container was sprayed with ethanol (EtOH) and aseptically transferred to a sterile fume hood to begin passaging. We retrieved the confluent cells from a 37°C humidified incubator set to a 5% CO₂ level. The medium was aspirated from the flask and the cells were washed with HBSS/PBS two times. This salt solution was aspirated; the cells were trypsinized, and then transferred into a sterile centrifuge tube with medium. Depending on the cell line, we centrifuged the suspension at rpm (revolutions per minute) values ranging from 300 rpm to 1200 rpm for 5-8 minutes. The supernatant was aspirated from the centrifuge tube, and the cells were resuspended in new medium. We transferred a portion of the cell suspension into a T-25 or T-75 flask with fresh media. The remainder of the cell suspension was used to coat the modified alginate microbeads. The flask with cultured cells was placed into the 37°C humidified incubator. We examined the cells for confluency daily using an inverted phase contrast microscope. If the cells were not confluent, we replaced the cell medium and returned the flask to the 37°C incubator overnight. However, if the cell colonies were large and highly dense, we trypsinized the cells and passaged them again by repeating the aforementioned protocol.

Immunocytochemistry of Fibronectin Coated Microbeads

The alginate hydrogel microbeads, including a second set without the fibronectin coating, were washed three times with 1X PBS and fixed for 15 minutes with 4% Paraformaldehyde (PFA). The microbeads were washed again three times with PBS after fixation and incubated for 1 hour at room temperature. We prepared a 20% Donkey serum (DS) solution by combining 60µL of DS with 240µL PBS to create a 300µL stock. The three sets of microbeads were

blocked with 100 μ L of 20% DS for 30 minutes at room temperature to prevent non-specific binding. We created a 1:100 dilution of the primary antibody by combining 3 μ L of the fibronectin antibody with 297 μ L of Bovine Serum Albumin (BSA). This yielded a 300 μ L stock. The 1:100 primary antibody was centrifuged at 4°C for 5-10 minutes, and the pellet was discarded. The supernatant containing the purified primary antibody was used to coat the microbeads. All microbeads were treated with the 1° antibody except for the fibronectin-coated control microbeads that served as the no 1° antibodies control to test for non-specific secondary antibody binding. They were washed three times with 1X PBS. The donkey anti-rabbit Cy2-conjugated secondary antibody was prepared and centrifuged at 4°C for 5-10 minutes to separate any non-solubilized material. The microbeads were incubated with the 2° antibody for 1-2 hours at room temperature. Before mounting onto glass slides, the microbeads were washed several times with 1X PBS and allowed to dry overnight with Fluoro-gel mounting solution. Images were captured using a CellObserver Z1 and an AxioCam MR digital camera driven by AxioVision software (all Carl Zeiss).

Attachment of Cells to Outer Membrane of 3-D Alginate Microbeads

Using a pipette, the gelatin, FBS, PLL, and fibronectin surface coats were aspirated from the well cell culture plates containing the alginate microbeads. MESCs, NIH 3T3 Fibroblast, and SIMS cell lines were passaged according to the protocol described in the previous section. Following centrifugation and resuspension in fresh media, the cells were added to the PBS-washed microbeads. Using an inverted microscope, we manually counted the number of cells to quantify the average number of cells adhered to the outer surface of the microbeads after 24 hours and 72 hours.

Results

Mouse Embryonic Stem Cells as a Model Cell Line

We used mESCs for model cells as a preliminary approach to using acinar cells. We found that mESCs had a propensity to preferentially attach to themselves and form embryoid bodies when suspended in media without a gelatin-treated tissue culture plate (Figure 36).

Therefore, we decided to test for cell adhesion using 3T3 fibroblast cells as a model line because they naturally express fibronectin surface receptors – which would facilitate their attachment to fibronectin-coated microbeads.

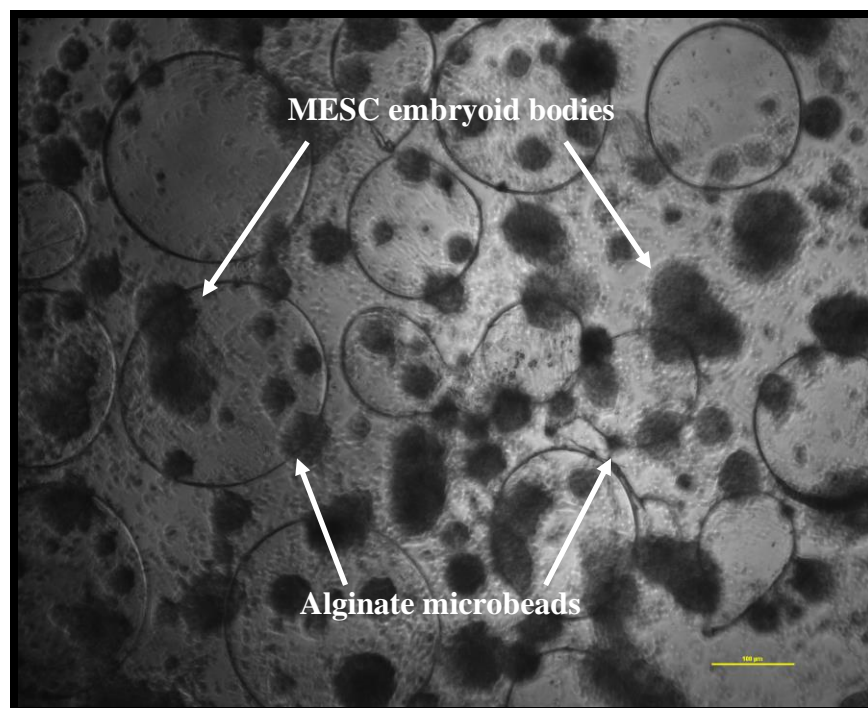


Figure 36: PLL-coated Alginate Microbeads with MESC
With PLL as our strongest surface coat, MESC still preferred to aggregate into embryoid bodies during differentiation.

Effect of Multilayer Surface Coats on 3T3 Fibroblast Cell Adhesion

To optimize cell adhesion, we investigated the effect of applying multilayer surface coats to our alginate microbeads. Outer surface coats of FBS and gelatin were not entirely effective in promoting adhesion. However, the results we obtained with PLL as an outer surface coat were more substantial. We discovered that there was no profound difference between cell attachment with the multilayer surface coat and the single surface coat of PLL (Figure 37). As a result, for efficiency, we proceeded to optimize cell adhesion by using only a single outer surface coat of PLL.

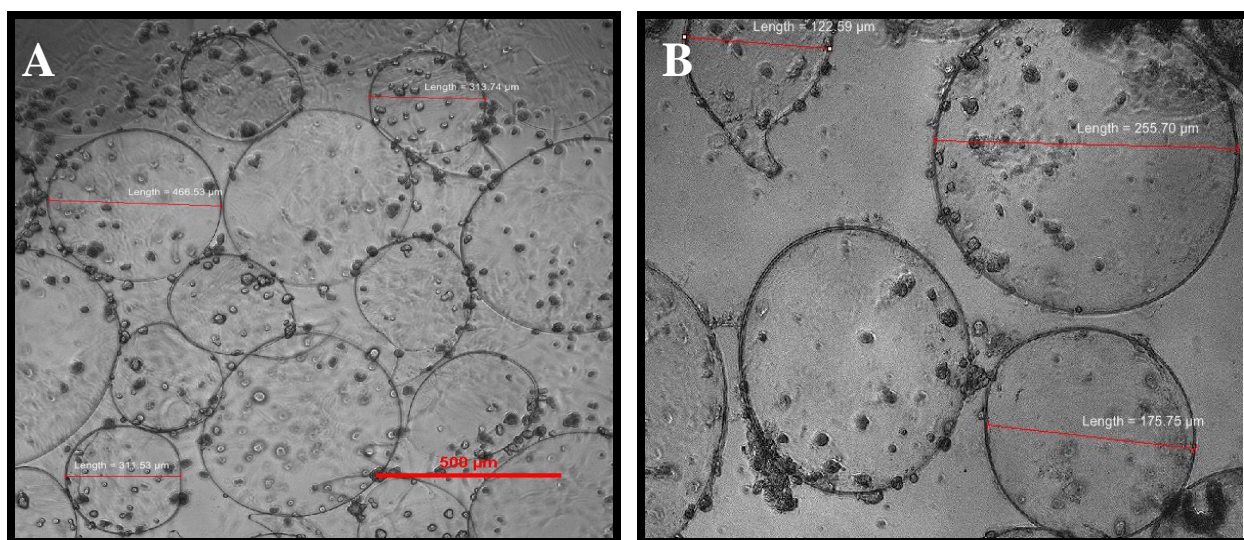


Figure 37: Effect of Cell Adhesion using Multilayer Surface Coats
(a) 3T3 fibroblast cells adhered to low MW PLL-0.15% alginate-PLL-coated microbeads
(b) 3T3 fibroblast cells adhered to PLL-coated microbeads

Optimization of Fibroblast Cell Adhesion using Different Surface Coats

Although FBS promoted cell adhesion initially, we wanted to determine the feasibility of increasing the density at which the cells were adhering. Therefore, we optimized cell adhesion using gelatin. Gelatin was not able to induce cell attachment to the extent that we had

anticipated. Fortunately, PLL and fibronectin turned out to be fairly effective as outer surface coats (Figure 38).

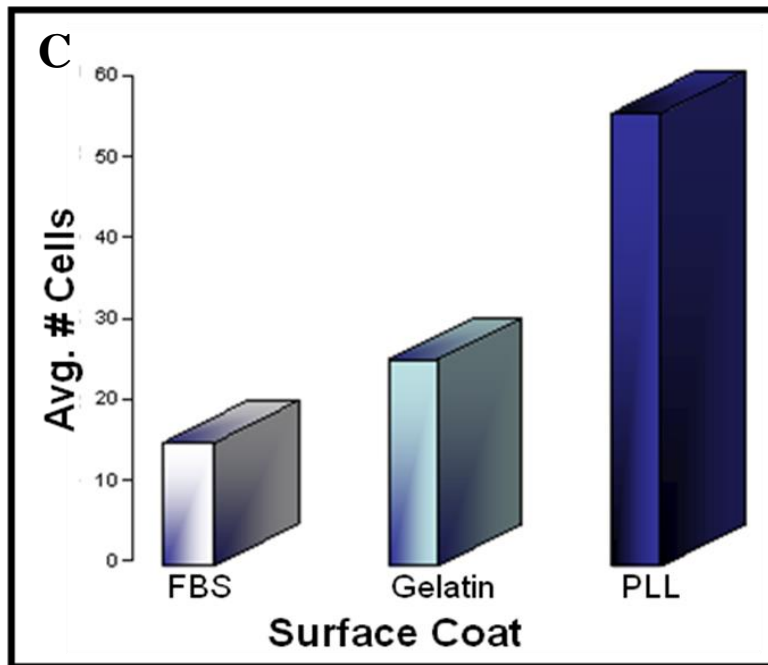
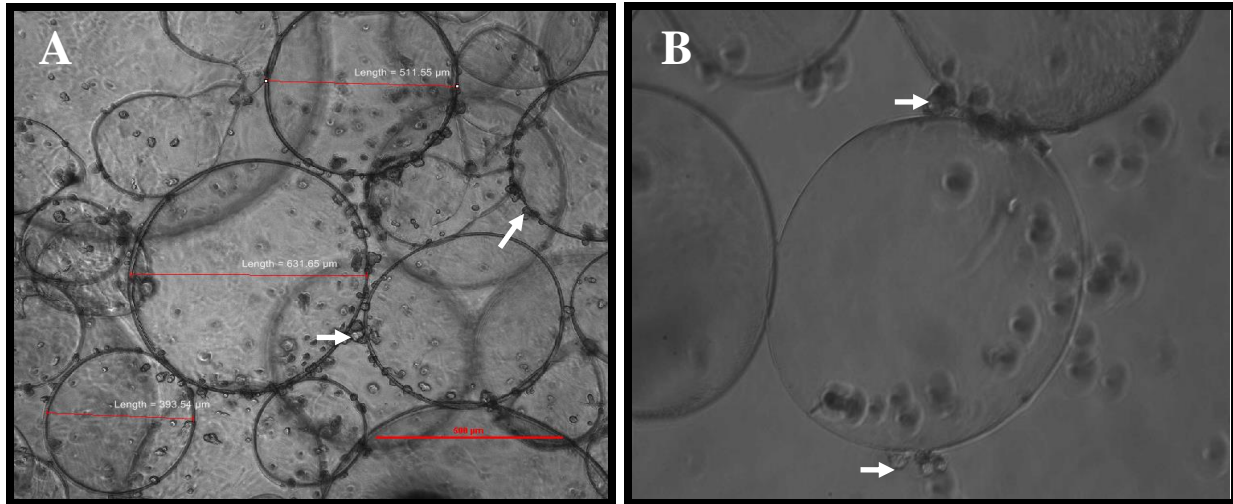


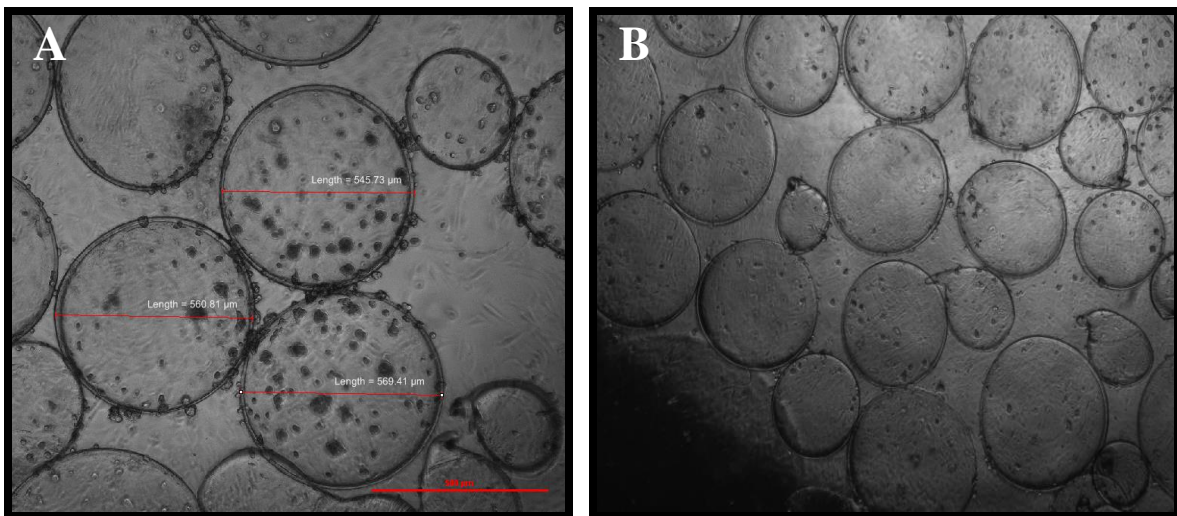
Figure 38: Effect of Different Surface Coatings on Cell Attachment

(a) 3T3 fibroblast cells adhered to PLL-coated microbeads (b) 3T3 fibroblast cells adhered to fibronectin-coated microbeads (c) Chart presenting the efficacy of FBS, gelatin, and PLL outer surface coats for MSCs.

Effect of Incubation Time on Fibroblast Cell Adhesion

Over time, we found that the fibroblast cells gradually lost their affinity for the outer PLL surface coat (Figure 39). When quantified at 24 hours, the average number of cells adhered to the visible surface of the microbeads was approximately 55 cells per microbead. When the microbeads were quantified 48 hours later, the amount of cells on the surface decreased. On average, we determined the number of cells present on the surface of the microbeads at 72 hours to be about 25 cells per microbead. These observations led us to assume that PLL was incapable of promoting sustained cell adhesion.

We attempted to optimize cell adhesion using an outer surface coat of fibronectin. When cells were seeded on the fibronectin-coated or non-coated beads, at first, we discovered that the cells did not display as strong of an attraction to the coat as we had expected. However, over a period of five days, we realized that the fibronectin coat was capable of sustaining the same level of cell adhesion it had initially (Figure 40). This phenomenon was not apparent with the PLL surface coating.



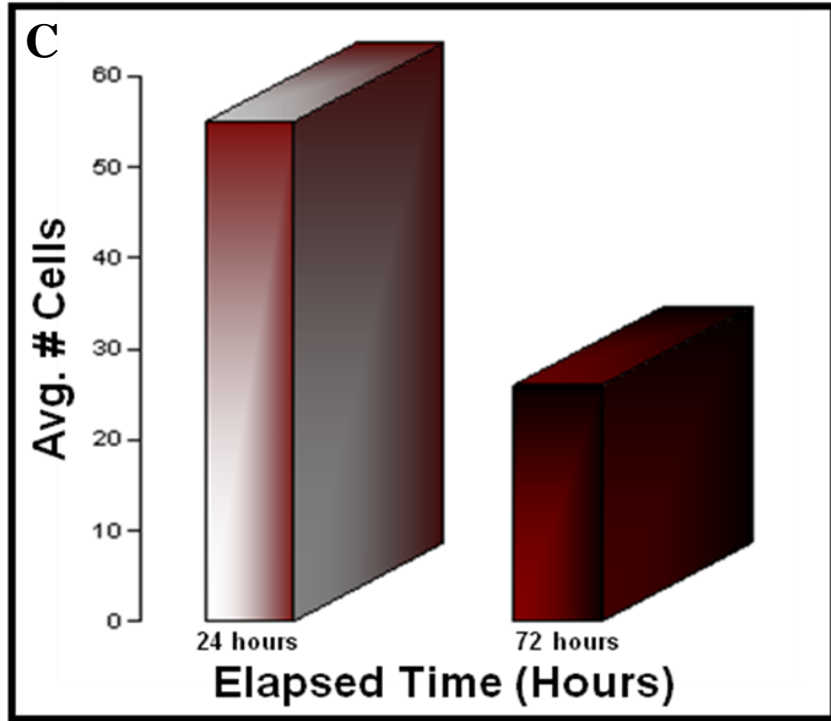


Figure 39: Effect of Time on Fibroblast Cell Adhesion to PLL-coated Microbeads

(a) PLL-coated microbeads quantified at 24 hours display an average of 55 cells per microbead. (b) PLL-coated microbeads quantified at 72 hours display 25 cells per microbead. (c) Diagram portraying decline in the number of cells adhered to the PLL-coated microbeads over a period of 72 hours.

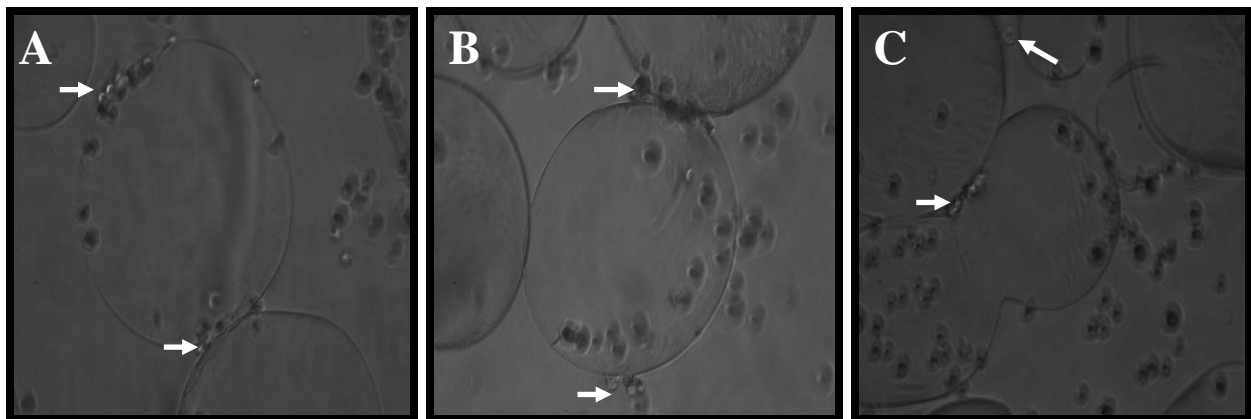


Figure 40: Effect of Time on Fibroblast Cell Adhesion to Fibronectin-coated Microbeads

(a) Fibronectin-coated microbeads after 24 hours. (b) Fibronectin-coated microbeads after 72 hours. (c) Fibronectin-coated microbeads after 120 hours (5 days later).

Sybr Green and Rhodamine-Phalloidin Fluorescent Staining

Sybr green and phalloidin staining were performed on the cells to detect the presence of cells attached to the beads by fluorescent microscopy. The Sybr green and rhodamine-phalloidin stains indicated that the 3T3 fibroblast cells were attached to the alginate microbeads with an outer surface coat of PLL (Figure 41a). The green stain (Sybr green) was used to stain the cell nuclei of the cell; and the red (Rhodamine-Phalloidin) was use to stain for the cytoskeleton. These results merely confirmed that cell adhesion to the PLL-coated microbeads were evident after a period of 24 hours.

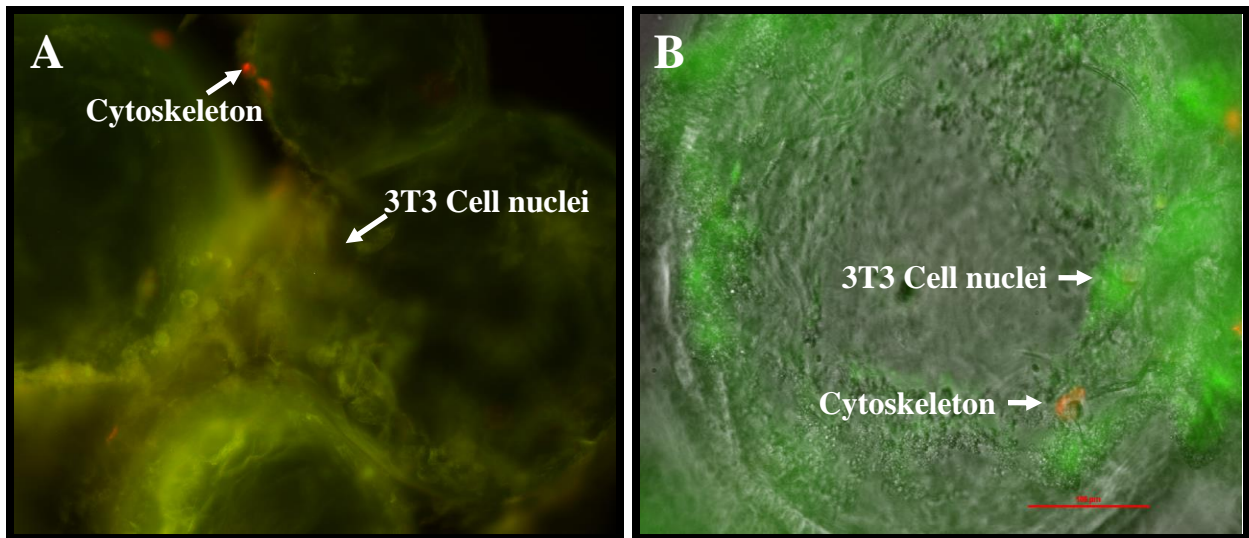


Figure 41: Sybr green and Rhodamine-Phalloidin fluorescent stain on PLL-coated Microbeads with 3T3 Fibroblast Cells

(a) Stained PLL-coated microbeads at a magnification of 10X. (b) Stained PLL-coated microbeads at a magnification of 20X. The red fluorescence depicts the cytoskeleton of the cell, and the green fluorescence depicts the cell nuclei.

Immunocytochemistry of Fibronectin-Coated Microbeads

We performed immunocytochemistry on the fibronectin-coated microbeads to verify that the fibronectin was adhering to the surface of the alginate microbeads effectively. Our results indicated that even after multiple washes, the fibronectin was still present on the outer surface of our microbeads (Figure 42a). To provide evidence supporting this conclusion, we provided two controls of the microbeads. The first control involved applying the primary, as well as the secondary antibodies to alginate microbeads without a fibronectin surface coat. The second control involved fibronectin-coated microbeads without the primary antibody, but with the secondary antibody. We did not observe any fluorescence after imaging the second control (Figure 42b). Therefore, we were able to deduce that the secondary antibody could not attach without the fibronectin antibody being present on the microbead initially. It also indicated that the blocking step we performed with DS was effective; and as a result the antibody could not non-specifically attach to the beads. The alginate microbeads do not appear to be spherical and intact because the coverslip flattened them. To surmount this problem, spacers must be used in the future to maintain the integrity and shape of the microbeads while imaging.

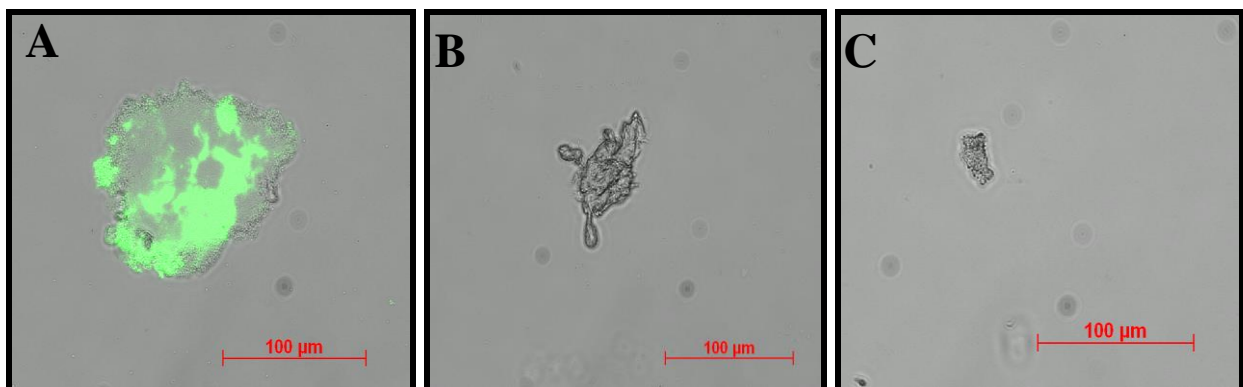


Figure 42: Immunostaining of Fibronectin-coated Microbeads (20X Magnification)

(a) Fibronectin-coated microbeads with fibronectin primary antibody. (b) Alginate microbead without initial fibronectin surface coat (control 1). (c) Fibronectin coated microbead without fibronectin primary antibody (control 2).

Optimization of SIMS Cell Adhesion Using Different Surface Coats

We progressed to use the salivary SIMS cell line to investigate cell adhesion using a variety of surface coats. The surfaces of the microbeads were modified with monolayers of PLL, gelatin, FBS, and fibronectin (FN). After 24 hours of incubation, FBS appeared to be the most effective surface coat in promoting cell attachment (Figure 43a). Large clusters of cells were conspicuously adhered to the outer membrane of the FBS-coated microbeads. Gelatin and PLL seemed to facilitate cell adhesion at similar levels, although not to the extent that FBS did. However, fibronectin fared worse than all of the other surface coats in this experiment because it did not adequately promote attachment of the SIMS cells.

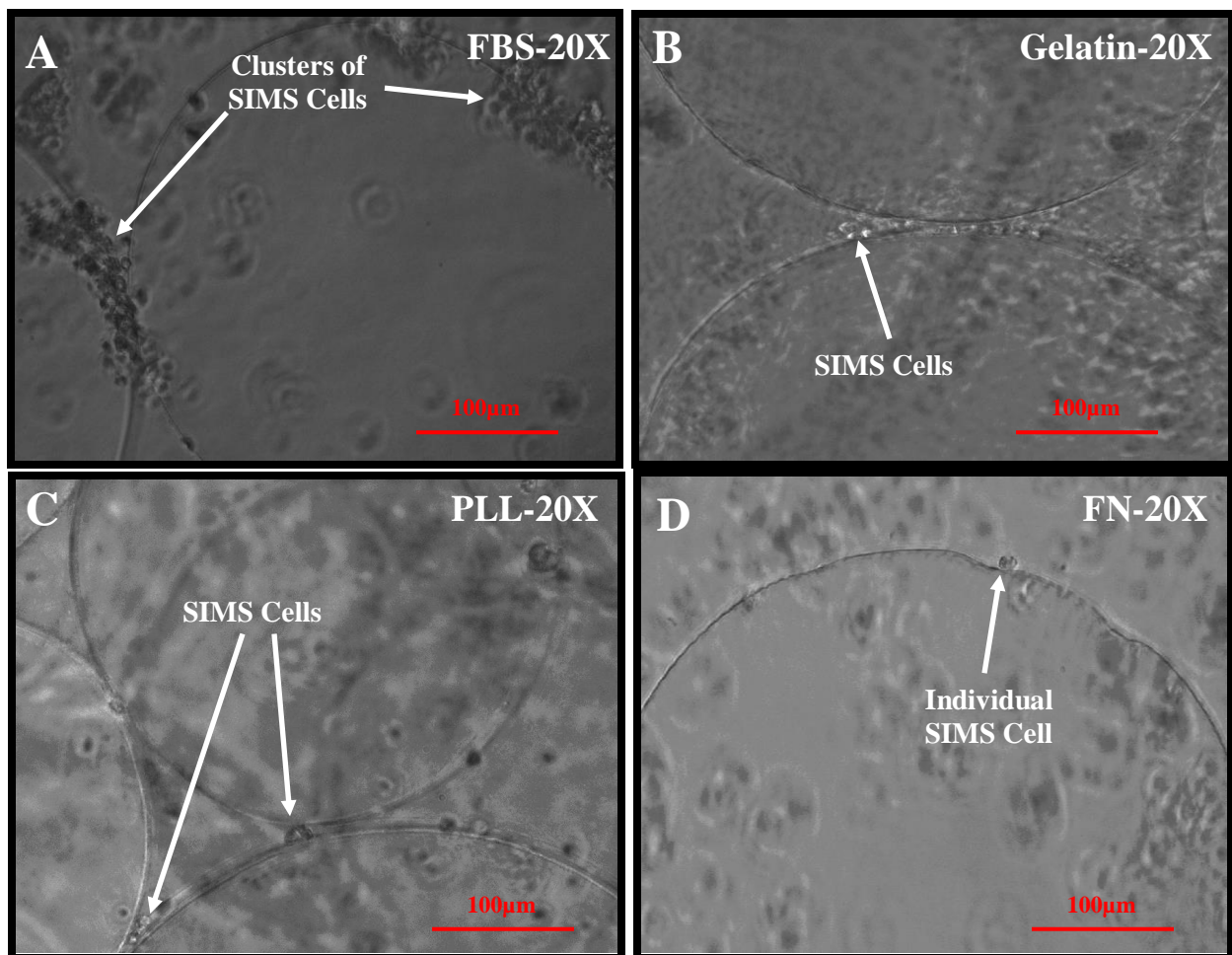


Figure 43: SIMS Cells Adhered to Different Surface Coats (20X Magnification)

(a) FBS-coated microbeads (b) Gelatin-coated microbeads (c) PLL-coated microbeads (d) FN-coated microbeads

Discussion

We discovered that mESCs preferred to form embryoid bodies rather than adhere to the outer surface coats we provided for them. Therefore, we proceeded to use 3T3 fibroblast cells as our model cell line for our preliminary experiments in optimizing cell adhesion. We found that PLL was an effective surface coat in promoting an initial strong adherence of cells to the microbeads. However, PLL was not shown to favor sustained cell adhesion. The 3T3 fibroblast cells were detaching from the PLL coated microbeads after a period of 72 hours possibly because the PLL was dissolving from the surface of the microbeads. Another possibility suggested that the fibroblast cells were expressing a type of proteolytic activity and were degrading the PLL surface coat. To confirm this hypothesis, a Western blot must be used to detect the presence of proteases, and perhaps perform these assays in the presence of additional protease inhibitors to analyze the source of the cells' weakened affinity for PLL.

Therefore, we decided to optimize sustained cell adhesion by applying a surface coat of fibronectin to replace PLL. Our results indicated that although fibronectin was effective in facilitating cell adhesion for a longer period of time, the cells did not adhere to fibronectin to the extent that they adhered to PLL. PLL had a stronger affinity for the cells initially because its positively charged amine groups attracted well to the negative charge present on the cell wall.

We were not sure why the cells did not attach to the fibronectin coat as strongly as we had anticipated. So we performed immunocytochemistry on the fibronectin-coated microbeads to detect whether the fibronectin was present on the outer surface. According to our results, the fibronectin was attaching to the alginate microbeads fairly well. The two controls that we used confirmed our observation. Our first control consisted of performing the protocol on alginate microbeads without a fibronectin surface coating. Our second control consisted of fibronectin-

coated microbeads without the primary fibronectin antibody. This was done to ensure that the secondary antibody required the primary fibronectin antibody to attach initially. Since we discovered that the 3T3 cells adhered to the fibronectin-coated microbeads, we decided to conduct studies that optimized cell adhesion using SIMS salivary cells.

The experiments that we performed with the SIMS cell line indicated that the efficacy of the surface coats was dependent on the cell type being used. FBS, one of our weakest surface coats when used to link 3T3 fibroblast cells to the microbeads, turned out to be our strongest surface coat when used with SIMS cells. On the other hand, fibronectin, which was able to promote a sustained cell adhesion in 3T3 fibroblasts, was actually our weakest surface coat altogether because it did not effectively facilitate adhesion of the SIMS cells. There were only a few isolated SIMS cells apparent on the outer surface of the fibronectin-coated microbeads. Further evidence supporting our hypothesis that the surface coats were cell-type dependent came from observations with PLL. In previous experiments, PLL initially helped anchor the 3T3 fibroblast cells to the microbeads strongly. It did this to a greater extent than FBS. However, when compared to its use with SIMS cells, it only promoted cell adhesion on a few locations on the surface of the microbeads. The compilation of results that we obtained while attempting to optimize SIMS cell adhesion suggested that the efficacy of the surface coats depended mainly on the cell line being used.

Conclusion

In this work, we investigated several different strategies for the development of an artificial scaffold for salivary gland acinar cells using alginate as a scaffold material. Initially, we were able to demonstrate that sodium alginate, when cross-linked with calcium chloride, was able to form an irreversible gel matrix capable of resembling natural biological tissue. However, fabricating alginate tissue constructs in the shape of microtubes by using the microfluidic approaches discussed in chapter 1 was not entirely efficient. The techniques that we employed were highly inconsistent and tedious. Since the ultimate goal of the project in chapter 1 was to create hydrogel constructs that could further be arranged into a salivary gland unit, we decided to move on to discover techniques that were more effective.

In chapters 2, we attempted a novel technique to generate alginate hydrogel nanofibers on more of a consistent basis. The electrospinning approach proved to be rather successful in fulfilling this short-term goal. We discovered that by altering several parameters, including the molecular weight and overall concentration of the solution, we could optimize the morphology of the nanofiber scaffolds. After further optimization of the aforementioned parameters, the resultant nanofibers produced will be able to mimic the architecture and topography of the biological extracellular matrix found *in vivo* of a salivary gland.

In chapter 3, we sought to develop alginate hydrogel beads that mimicked the shape of salivary gland acini. We were able to fabricate alginate hydrogel microbeads via the electrodroplet technique. By modifying the surfaces of the hydrogel microbeads to promote cell adhesion, we found that we were able maximize the number of cells that could bind with the use of a poly-L-lysine coat. However, the cells did not attach for long periods of time with this coating. Modifying the beads with fibronectin resulted in a sustained attachment of cells to the

microbeads, however the cells did not attach as strongly as they did with the PLL surface coat. An alternative approach to improve the adhesive properties of the cells would be to use fibronectin peptides as a surface coating to increase the number of binding sites.

Although these studies using mouse fibroblasts (NIH 3T3 cells) and SIMS cells provide a proof of concept for our approach, a future goal of this project is to optimize attachment of salivary gland cells to the alginate microbeads. We have demonstrated that the SIMS salivary gland cell line does attach to the modified alginate microbeads. However, the SIMS cells do not organize into a polarized cell layer. It may be that we need to provide a signal on the microbeads to induce polarization (i.e. collagen IV or laminin, which are proteins found on the basement membrane). In the meantime, the SIMS cells that are attached to the outside of the microbeads will be polarized in such a way that the cells will be able to secrete in this arrangement. Although the cells will not be able to distinguish between the basal and apical sides at this point, with this preliminary arrangement, the saliva that is produced will be collected into a biocompatible scaffold compartment consisting of ducts that extend into the mouth. The artificial ducts of the compartment will then be responsible for transporting the saliva produced by the acinar cells to various parts of the oral cavity.

Ultimately, we would like to create a spherical scaffold that would facilitate the organization of the cells to create tissue constructs that emulate the acinar structures present in salivary glands. To accomplish this, we would need to encapsulate the cells on the inside of the beads to replicate the tissue structure of the real gland present *in vivo* (Figure 34). By equipping the microbeads with a basement membrane and other signaling factors, the cells will be able to establish these apical and basal sides.

In the future, we will work on further optimization of these methods to develop tissue constructs that best simulate the mammalian salivary gland. After we seed acinar cells onto our alginate hydrogel constructs, allow the cells to organize into functional units, assay for expression of salivary acinar differentiation markers, we can ultimately assemble the hydrogel constructs (microbeads, nanofibers, and microstrands) to engineer a functioning artificial salivary gland. However, one of the major challenges that we will face is how to assemble the acinar and ductal tissue constructs *in vitro* to best emulate the structure of the mammalian salivary gland. The complexity of the biological salivary gland makes this aspect quite difficult. Furthermore, once we find innovative ways to connect the tissue constructs, their functionality would first need to be tested *in vitro*, and then in a model organism (e.g. *Mus musculus* – mouse). Before the functioning salivary gland can be implanted into patients with hypofunction, we would need to replace our mouse cell lines with human acinar cells and seed them onto the alginate scaffolds. Nevertheless, once we breach through the technical problems and obstacles that arise in this project, we will ultimately be able to bioengineer a functioning salivary gland to treat patients suffering from xerostomia.

References

- Ahearne, M., Yang, Y., Haj, A.J, Then, K.Y, Liu, K.K. Characterizing the viscoelastic properties of thin hydrogel-based constructs for tissue engineering applications. *J. R. Soc. Interface*, **2**, 455 – 463, 2005.
- Aframian, D.J., Palmon, A. Current status of the development of an artificial salivary gland. *Tissue Engineering*, **14**, 1 – 12, 2008.
- Akane, T., Toshiaki, N. Acceleration of wound healing by gelatin film dressings with epidermal growth factor. *Current Applied Physics*, **5**, 463 – 467. 2005.
- Atashi, A., Nadri, S., Maryam, H., Soleimani, M. Role of poly-L-lysine-coated plates and fetal calf serum concentration in sheep chondroprogenitor cell culturing. *Journal of Artificial organs*, **12**, 118 – 122, 2009.
- Atkinson, J.C., and Wu, A.J. Salivary gland dysfunction: causes, symptoms, treatment. *J. Am. Dent. Assoc.* **125**, 409, 1994.
- Choi, Y.J., Noh, I. Media tissue regeneration of the hybrid expanded polytetrafluoroethylene vascular graft via gelatin coating. *Curr. Appl Phys*, **5**, 463 – 467, 2005.
- George, J.H.S. Engineering of fibrous scaffolds for use in regenerative medicine. *Department of Materials London*, 1 – 200, 2009.
- Dodds, M.W.J, Johnson, D.A, Yeh, C. Health benefits of saliva: a review. *Journal of Dentistry*. **33**, 223-233, 2005.
- Gerecht-Nir S, Cohen S, Ziskind A and Itskovitz-Eldor J. 3-D porous alginate scaffolds provide a conducive environment for the generation of well vascularized embryoid bodies from human embryonic stem cells. *Biotechnol Bioeng*. **88**, 313 – 320, 2004.
- Hayman E.G., Pierschbacher M.D., Suzuki S., Ruoslahti E. Vitronectin--a major cell attachment-promoting protein in fetal bovine serum. *Exp Cell Res*, **160**, 245 – 258, 1985.
- Hou, Q., Buttery, D.K., Freeman, R., Shakesheff, K.M. Surface engineering of alginate scaffolds for the attachment of embryonic stem cells. *European Cells and Materiasl*, **10**, 66, 2005.
- Kameoka, J., Orth, R., Yang, Y., Czaplowski, D., Mathers, R., Coates, G., Craighead, H.G. A scanning tip electrospinning source for deposition of oriented nanofibres. *Nanotechnology*, **14**, 1124 – 1129., 2003.
- Kim, P., Kwon, W., Park, C., Lee, S.H., Kim, S.M., Suh, K.Y. Soft lithography for microfluidics: A Review. *Biochip Journal*, **2** (1), 1 – 11, 2008.

- Lee, S., Spencer, N.D., Adsorption properties of poly (L-lysine)-graft-poly(ethylene glycol) (PLL-g-PEG) at a hydrophobic interface: influence of tribological stress, pH, salt concentration, and polymer molecular weight. *Langmuir*, **24**, 9479 – 9488, 2008.
- Liu, C., Xia, Z., Czernuszka, J.T. Design and Development of Three-Dimensional Scaffolds for Tissue Engineering. *Chemical Engineering Research and Design*. **85**, 1051 – 1064, 2007.
- Lu, J.W., Zhu, Y.L., Guo, Z.X., Hu, P., Yu, J. Electrospinning of sodium alginate with poly(ethylene oxide). *Science Direct*, **47**, 8026 – 8031, 2006.
- Nie, H., He, A., Zheng, J., Xu, S., Li, J., Han, C. Effects of chain conformation and entanglement on the electrospinning of pure alginate. *Biomacromolecules*, **9**, 1362 – 1365, 2008.
- Ning.F., Guo. YI, Tang, J., Zhou, J., Zhang, H., Lu., W., Gao, Y., Wang., L. Pei, D. Duan, Y., Jin, Y. Differentiation of mouse embryonic stem cells in dental epithelial-like cells induced by ameloblasts serum-free conditioned medium. *Biochem Biophys Res Commun*. **394**, 342 – 347, 2010.
- Orive, G, Tam, S.K, Pedraz, J.L., Halle, J. Biocompatibility of alginate–poly-l-lysine microcapsules for cell therapy. *Biomaterials*. **27**, 3691-3700, 2006.
- Porter, S.R., Fedele, S., Hababb, K.M. Xerostomia in head and neck malignancy. *Oral Oncology*. 2010.
- Taylor, G., Disintegration of Water Drops in an Electric Field. *Proceedings of the Royal Society of London Series A, Mathematical and Physical Sciences*, **280**, 383 – 397, 1964.
- Teo, W.E, He, W., Ramakrishna, S. Electrospun scaffolds tailored for tissue-specific extracellular matrix. *Biotechnology Journal*, **1**, 918 – 929, 2010.
- Todaro, G.J., Green, H. Quantitative studies of the growth of mouse embryo cells in culture and their development into established lines. *Journal of Cell Biology*, **17**, 299 – 313, 1963.
- Topuz, F., Okay, O. *Reactive and Functional Polymers*. Macroporous hydrogel beads of high toughness and superfast responsivity. **69**, 273 – 280, 2009.
- Wei, C., Larsen, M., Hoffman, M.P., Yamada, K.M. Self-organization and branching morphogenesis of primary salivary epithelial cells. *Tissue Engineering*, **13**, 721 – 735, 2007.
- Wells, J.T, Lucey, M.R., Said, A. Hepatitis C in transplant recipients of solid organs, other than liver. *Clinics in Liver Disease*. **10**, 901 – 917, 2006.
- Zhong, X.H., Kim, K.S., Fang, D.F., Ran, S.F., Hsiao, B.S., Chu, B. Structure and process relationship of electrospun bioadsorbable nanofiber membranes. *Polymer*, **43**, 4403 – 4412, 2002.

